Article

Molecular Cell

Gamblers: An Antibiotic-Induced Evolvable Cell Subpopulation Differentiated by Reactive-Oxygen-Induced General Stress Response

Graphical Abstract

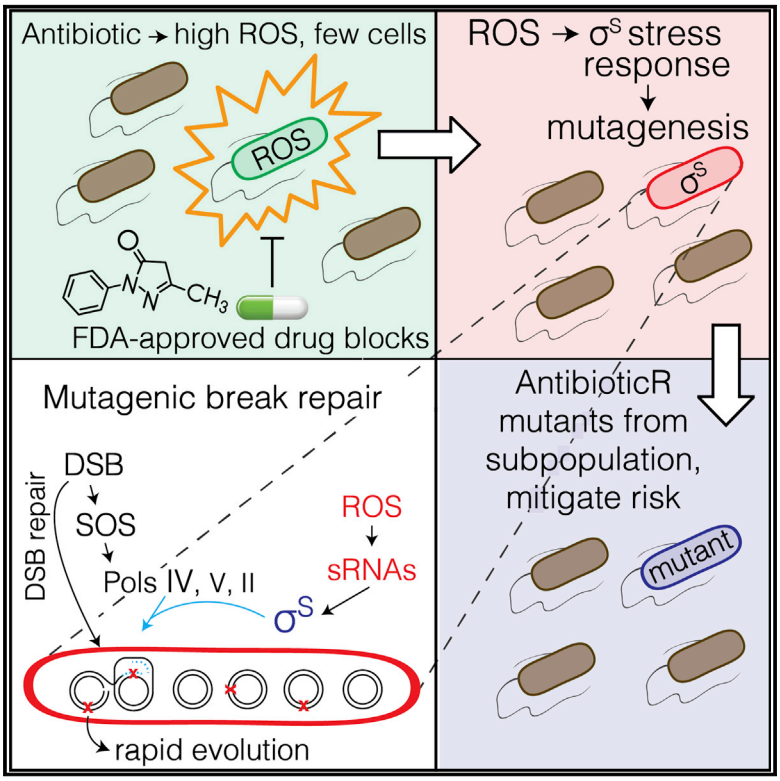

Highlights

- Antibiotic-induced mutable cell subpopulation generates resistant mutants
- Mitigates risk to most cells; reactive oxygen → σ^S stress response → gamblers
- FDA-approved drug blocks σ^S response and mutagenesis: anti-evolvability drug
- Multiple chromosomes needed: chromosome cooperation can allow rapid adaptation

Authors

John P. Pribis, Libertad García-Villada, Yin Zhai, ..., Lilach Hadany, P.J. Hastings, Susan M. Rosenberg

Correspondence

smr@bcm.edu

In Brief

Bacteria exposed to antibiotic acquire reactive oxygen in a transient "gambler" cell subpopulation that undertakes general stress response-induced mutagenic DNA break repair, evolves resistance to new antibiotics, and is inhibited by an FDA-approved drug that inhibits evolvability.

Pribis et al., 2019, Molecular Cell *74*, 785–800
May 16, 2019
https://doi.org/10.1016/j.molcel.2019.02.037

CellPress

Molecular Cell
Article

Gamblers: An Antibiotic-Induced Evolvable Cell Subpopulation Differentiated by Reactive-Oxygen-Induced General Stress Response

John P. Pribis,[1,2,3,4,5] Libertad García-Villada,[1,2,3,4,12] Yin Zhai,[1,2,3,4,12] Ohad Lewin-Epstein,[10] Anthony Z. Wang,[6] Jingjing Liu,[1,2,3,4] Jun Xia,[1,2,3,4] Qian Mei,[1,2,3,4,7] Devon M. Fitzgerald,[2,3,4] Julia Bos,[8,9,11] Robert H. Austin,[9] Christophe Herman,[1,3,4,5] David Bates,[1,3,4,5] Lilach Hadany,[10] P.J. Hastings,[1,4] and Susan M. Rosenberg[1,2,3,4,5,6,7,13,*]
[1]Department of Molecular and Human Genetics, Baylor College of Medicine, Houston, TX 77030, USA
[2]Department of Biochemistry and Molecular Biology, Baylor College of Medicine, Houston, TX 77030, USA
[3]Department of Molecular Virology and Microbiology, Baylor College of Medicine, Houston, TX 77030, USA
[4]The Dan L. Duncan Comprehensive Cancer Center, Baylor College of Medicine, Houston, TX 77030, USA
[5]Graduate Program in Integrative Molecular and Biomedical Sciences, Baylor College of Medicine, Houston, TX 77030, USA
[6]Department of Biochemistry and Cell Biology, Rice University, Houston, TX 77030, USA
[7]Systems, Synthetic, and Physical Biology Program, Rice University, Houston, TX 77030, USA
[8]Department of Physics, Princeton University, Princeton, NJ 08544-0708, USA
[9]Lewis Sigler Institute, Princeton University, Princeton, NJ 08544-0708, USA
[10]Department of Molecular Biology and Ecology of Plants, Tel-Aviv University, Tel-Aviv, Israel
[11]Present address: Bacterial Genome Plasticity, Institut Pasteur, 75015 Paris, France
[12]These authors contributed equally
[13]Lead Contact
*Correspondence: smr@bcm.edu
https://doi.org/10.1016/j.molcel.2019.02.037

SUMMARY

Antibiotics can induce mutations that cause antibiotic resistance. Yet, despite their importance, mechanisms of antibiotic-promoted mutagenesis remain elusive. We report that the fluoroquinolone antibiotic ciprofloxacin (cipro) induces mutations by triggering transient differentiation of a mutant-generating cell subpopulation, using reactive oxygen species (ROS). Cipro-induced DNA breaks activate the *Escherichia coli* SOS DNA-damage response and error-prone DNA polymerases in all cells. However, mutagenesis is limited to a cell subpopulation in which electron transfer together with SOS induce ROS, which activate the sigma-S (σ^S) general-stress response, which allows mutagenic DNA-break repair. When sorted, this small σ^S-response-"on" subpopulation produces most antibiotic cross-resistant mutants. A U.S. Food and Drug Administration (FDA)-approved drug prevents σ^S induction, specifically inhibiting antibiotic-promoted mutagenesis. Further, SOS-inhibited cell division, which causes multi-chromosome cells, promotes mutagenesis. The data support a model in which within-cell chromosome cooperation together with development of a "gambler" cell subpopulation promote resistance evolution without risking most cells.

INTRODUCTION

Antibiotic resistance is a world health threat and occurs both by uptake of resistance genes from other bacteria and mutation of resident genes. New mutations underpin resistance to diverse antibiotics and dominate the World Health Organization's "priority pathogens" (Magrini, 2017). Historically, resistance has been addressed with new antibiotics. A complementary approach could be to discover, then inhibit, molecular mechanisms that drive evolution of resistance (Al Mamun et al., 2012; Cirz et al., 2005; Rosenberg and Queitsch, 2014). This has succeeded in fungi (Cowen and Lindquist, 2005; Shekhar-Guturja et al., 2016), but not yet in bacteria. Antimicrobials both select resistant mutants and can induce their formation (Cirz et al., 2005; Gutierrez et al., 2013; Kohanski et al., 2010). Although their mechanisms of growth arrest are detailed, how antibiotics induce new mutations is poorly understood.

Fluoroquinolone antibiotics inhibit bacterial type-II topoisomerases and kill cells via DNA double-strand breaks (DSBs) (Drlica, 1999). Resistance, including to ciprofloxacin (cipro), occurs mostly by *de novo* mutation. Cipro exposure at so-called "sub-inhibitory" concentrations (below minimal inhibitory concentration [MIC]), which occurs in ecosystems and during therapies, both induces and selects cipro resistance (Cirz et al., 2005). A fluoroquinolone also induced resistance mutations to antibiotics not yet encountered (Kohanski et al., 2010)—antibiotic "cross" resistance. The mutagenesis required reactive oxygen species (ROS) induced by the drug (Kohanski et al., 2010), as does the antibiotic (killing) activity at higher MIC doses (Kohanski et al., 2007). ROS promote killing by oxidizing DNA bases, which

cause more lethal DNA breaks during repair (Foti et al., 2012), however, whether this underlies the ROS mutagenic activity is unknown.

Here, we show that low, sub-inhibitory doses of cipro induce transient differentiation of a small cell subpopulation with high ROS and σ^S general stress-response activity that generates cross-resistant mutants: a "gambler" subpopulation. We show that in gambler cells, ROS activate the σ^S response, which allows mutagenic repair of cipro-triggered DSBs—a novel signaling and differentiating role of ROS in mutagenesis. We also find a requirement for SOS-induced inhibition of cell division, causing multiple chromosomes per cell. The findings imply a highly regulated, transient differentiation process and support a model in which within-cell chromosome cooperation together with development of a transient gambler subpopulation drive evolution of resistance to new antibiotics without risk to most cells.

RESULTS

Cipro-Induced Mutagenesis

We developed two assays for cipro-induced mutagenesis without cipro selection of the mutants (Figure 1A). In both assays, strains are grown in liquid, each with cipro at its minimum antibiotic concentration (MAC, final colony-forming units [CFU] are 10% of those of no-drug cultures) (Lorian and De Freitas, 1979). These are "low-dose" and "sub-inhibitory" relative to MICs (CFU $\leq 10^{-4}$ of untreated cells). Table S1 shows MACs and MICs for all strains assayed (wild-type MAC, 8.5 ng/mL). Cells are then removed from cipro and plated selectively for colonies resistant to rifampicin (RifR) or ampicillin (AmpR) antibiotics (Figure 1A), and mutation rates are estimated (STAR Methods). RifR arises by specific base-substitutions in the *rpoB* gene (Figure S1A), and AmpR arises by *ampD* null mutations in engineered *Escherichia coli* (Petrosino et al., 2002) (Figures S1B and S1C; STAR Methods). Strikingly, cipro increased RifR and AmpR mutation rates 26- and 18-fold above no-cipro rates (Figure 1B; Table S2 for all mutation rates). The RifR or AmpR mutants are not selected in sub-inhibitory cipro and are at a slight but significant disadvantage (Figure 1C), implying that mutation, not selection of the mutants, is elevated by MAC cipro. Additional controls show negligible cell death in the low-dose cipro (Figures S1D and S2, other controls).

ROS-Dependent Mutagenesis Is σ^S-Dependent Mutagenic Break Repair

The cipro-induced mutagenesis requires ROS and is inhibited by ROS scavenging or preventing agents thiourea (TU) and 2,2′-bipyridine (BP) (Figure 1D; Table S2). The following data indicate that the ROS instigate a σ^S-licensed mutagenic DNA break-repair (MBR) mechanism triggered by cipro-induced DSBs.

MBR is regulated mutagenesis during repair of DSBs, requiring the SOS and σ^S responses (Figure 1E) (Fitzgerald et al., 2017), which causes mutations when cells are maladapted to their environments when stressed. Spontaneous DSBs induce the SOS DNA-damage response and are repaired by homology-directed DSB repair (HR repair, Figure 1E). SOS transcriptionally upregulates error-prone DNA polymerases (Pols) IV, V, and II; however, repair synthesis is non-mutagenic unless the σ^S response is also induced (Ponder et al., 2005; Shee et al., 2011) (Figure 1E). σ^S, by unknown means, allows formation or persistence of errors made by Pols IV, V, and II in DSB repair, causing mutations (Fitzgerald et al., 2017; Ponder et al., 2005; Shee et al., 2011) near DSBs (Shee et al., 2012).

Most cipro-induced *ampD* and *rpoB* mutagenesis requires MBR proteins (Figure 1F; Table S2, raw rates), RecA, RecB, and RuvC (DSB-repair), SOS- and σ^S-response activators, and SOS-upregulated DNA Pols IV, V, and II, implying a MBR-like mechanism. SOS non-inducible (*lexA*Ind) or Δ*rpoS* (σ^S-deficient) strains (Table S1) showed 87% ± 3% and 70% ± 9% decreases (AmpR and RifR combined, mean ±95% confidence interval [CI]). Thus, two stress responses and repair are required—SOS is not sufficient (Figure 1F; Table S2). Double SOS-, σ^S-defective mutants show no further reduction (Figure S1E), implying action in the same pathway, as do ROS and σ^S (Figures S1F, S1D, and S2). Neither cell death nor no-drug mutation rates differ between strains (Table S2). Thus, cipro-induced ROS-dependent mutagenesis occurs by the σ^S-dependent MBR pathway.

The mutagenesis also requires reparable DSBs. MAC cipro induced DSBs, quantified as fluorescent foci of GamGFP DSB-end-specific binding protein (Shee et al., 2013), 28 ± 9 times above spontaneous levels (mean ± SEM) (Figures 1G, S3A, and S4A). GamGFP binds DSB ends preventing HR repair (Shee et al., 2013) and also inhibited cipro induction of mutagenesis (Figure 1H; Table S2), indicating that reparable DSBs are required. RecBCD interacts specifically with DSB ends (Kuzminov, 1999), and its requirement (Figure 1F, *recB*) also implies the necessity of DSBs in the mutagenesis, supporting a MBR mechanism.

Special functional gyrase and topo IV mutant proteins that are not bound by cipro (Khodursky et al., 1995) block induction of mutagenesis (Figure 1I; Table S2), implicating cipro-induced DSBs and making "off-target" effects unlikely. Further, σ^E and R-loop-promoting proteins promote starvation-stress-induced MBR by promoting spontaneous DSBs (Gibson et al., 2010; Wimberly et al., 2013) (Figure 1E) and are not required for cipro-induced MBR (Figure S1G). These data imply an MBR mechanism with the DSBs not from spontaneous sources, but instead from cipro action on topoisomerases.

ROS Differentiate a Cell Subpopulation, Activate σ^S Response

We surveyed single log phase cells for ROS and stress-response induction by flow cytometry. At time "0," cipro is added in early log phase, and all log-specific assays are at 16 h unless stated otherwise. SOS reporter P_{sulA}*mCherry* at a non-genic chromosomal site (Nehring et al., 2016; Pennington and Rosenberg, 2007) revealed population-wide dose-dependent SOS induction (Figure 2A), with 208 ± 26 times more SOS-positive cells at the 8.5 ng/mL mutagenic MAC dose than without drug. Auto-fluorescence (Renggli et al., 2013) is negligible (Figures S4B–S4D).

Surprisingly, only a discreet cell subpopulation(s) showed strong ROS or σ^S induction. ROS, detected with dihydrorhodamine 123 dye (DHR) (Figure 2B) in log phase, appear in a distinct 20% ± 3% cell subpopulation (mean ± SEM). Similarly, high σ^S activity (*yiaG-yfp* fluorescence) (Al Mamun et al., 2012) occurred

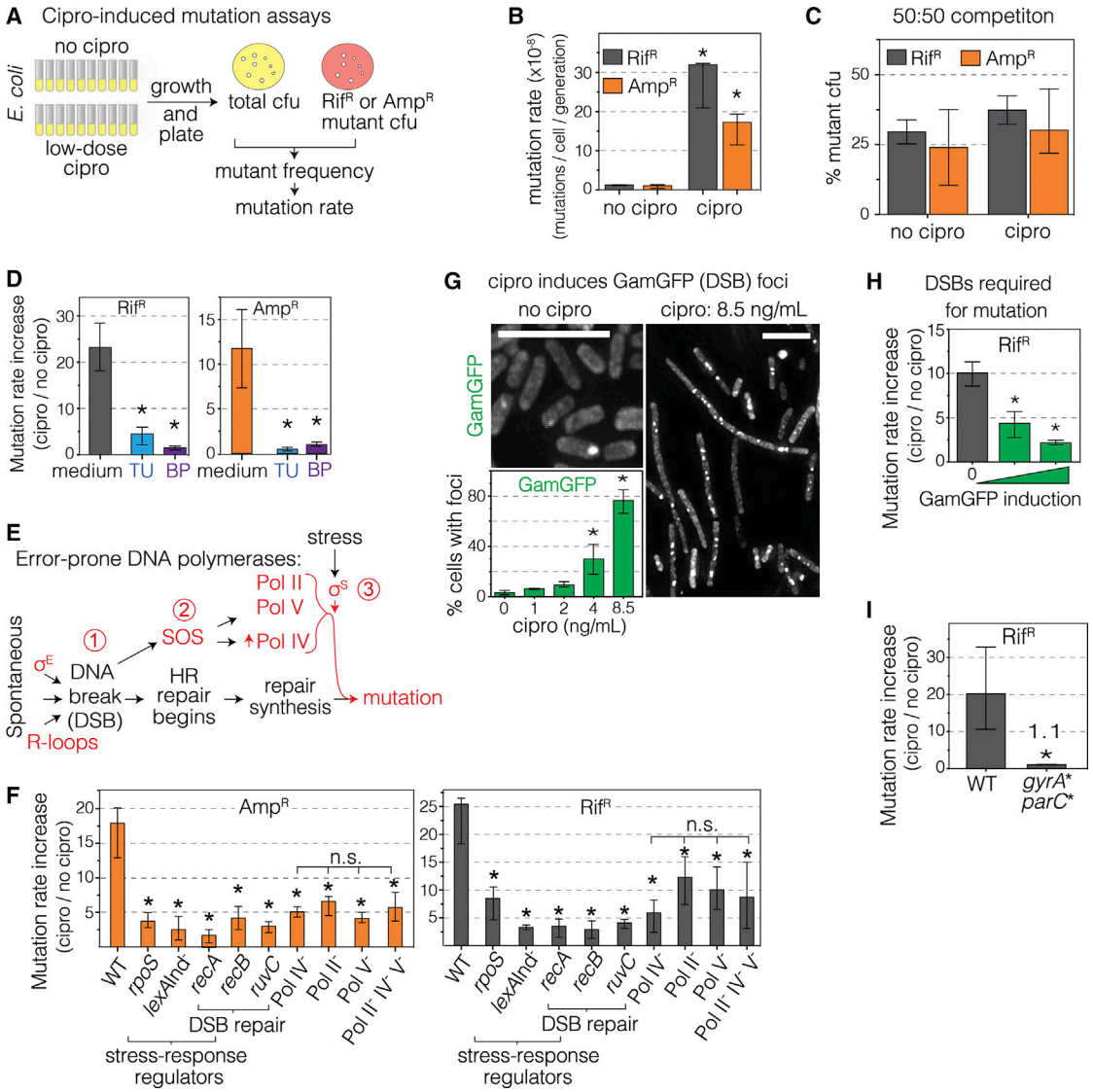

Figure 1. Cipro-Induced Mutagenesis via Cipro-Induced ROS and Mutagenic Break Repair

(A) Assays for base substitution (RifR) and null mutations (AmpR). Per STAR Methods with MAC cipro.

(B) MAC cipro induces RifR and AmpR mutagenesis (Figures S1A–S1C). Mean ± 95% confidence interval (CI), ≥3 independent experiments. *Differ from no cipro, $p < 0.001$, two-tailed Student's t test.

(C) Competition experiments: neither RifR nor AmpR mutants are selected in MAC cipro. Initial mixtures 50% mutant CFU. *rpoB* and *ampD* mutants are <50% after growth. AmpR, $p = 0.0098$; RifR, $p = 0.0014$, 1 sample t test indicating growth disadvantage. Means ± SEM, 3 independent experiments.

(D) ROS scavenger (thiourea [TU]) or preventer (2,2′-bipyridine [BP]) reduces mutation rates (Figure S2, additional controls). Fold induction of mutation rate (Table S2, raw rates). Means ± 95% CI, ≥3 experiments. *Different from medium, $p < 0.001$, one-way ANOVA with Tukey's post hoc test of natural-log transformed data.

(E) Starvation-stress-induced mutagenic break repair (MBR), reviewed by Al Mamun et al. (2012) and Fitzgerald et al. (2017) and in Results.

(F) Cipro-induced mutation requires MBR-pathway proteins. Mutants are grown at their respective MACs (Table S1). Means ± 95% CI, ≥4 experiments. *Different from wild-type (WT), $p < 0.001$, one-way ANOVA with Tukey's post hoc test of natural-log transformed data; n.s., not significant (Figure S1E, epistasis analyses; Table S2, raw rates).

(G) Cipro induces DSBs dose-dependently. Log phase, 8.5 ng/mL MAC. DSBs quantified as fluorescent foci of phage Mu GamGFP (Shee et al., 2013). Representative images. Scale bars, 5 μm. Mean ± SEM, 3 experiments. *Different from no Cipro, $p < 0.05$, one-way ANOVA with Tukey's post-hoc test.

(H) Reparable DSBs are required for cipro-induced mutagenesis. DSB-trapping GamGFP inhibits DSB repair (Shee et al., 2013) and cipro-induced mutagenesis. Means ± 95% CI, ≥3 experiments. *Different from no GamGFP, $p < 0.01$, one-way ANOVA with Tukey's post hoc test of natural-log transformed data.

(I) Cipro binding to its target type II topoisomerases is required for induction of mutagenesis. *gyrA* parC** encode functional gyrase and topoisomerase IV that are not bound by cipro. Means ± 95% CI, 3 experiments. *Different, $p < 0.001$, two-tailed Student's t test of natural-log transformed data.

See also Figures S1, S2, S3, and S4 and Tables S1, S2, and S4.

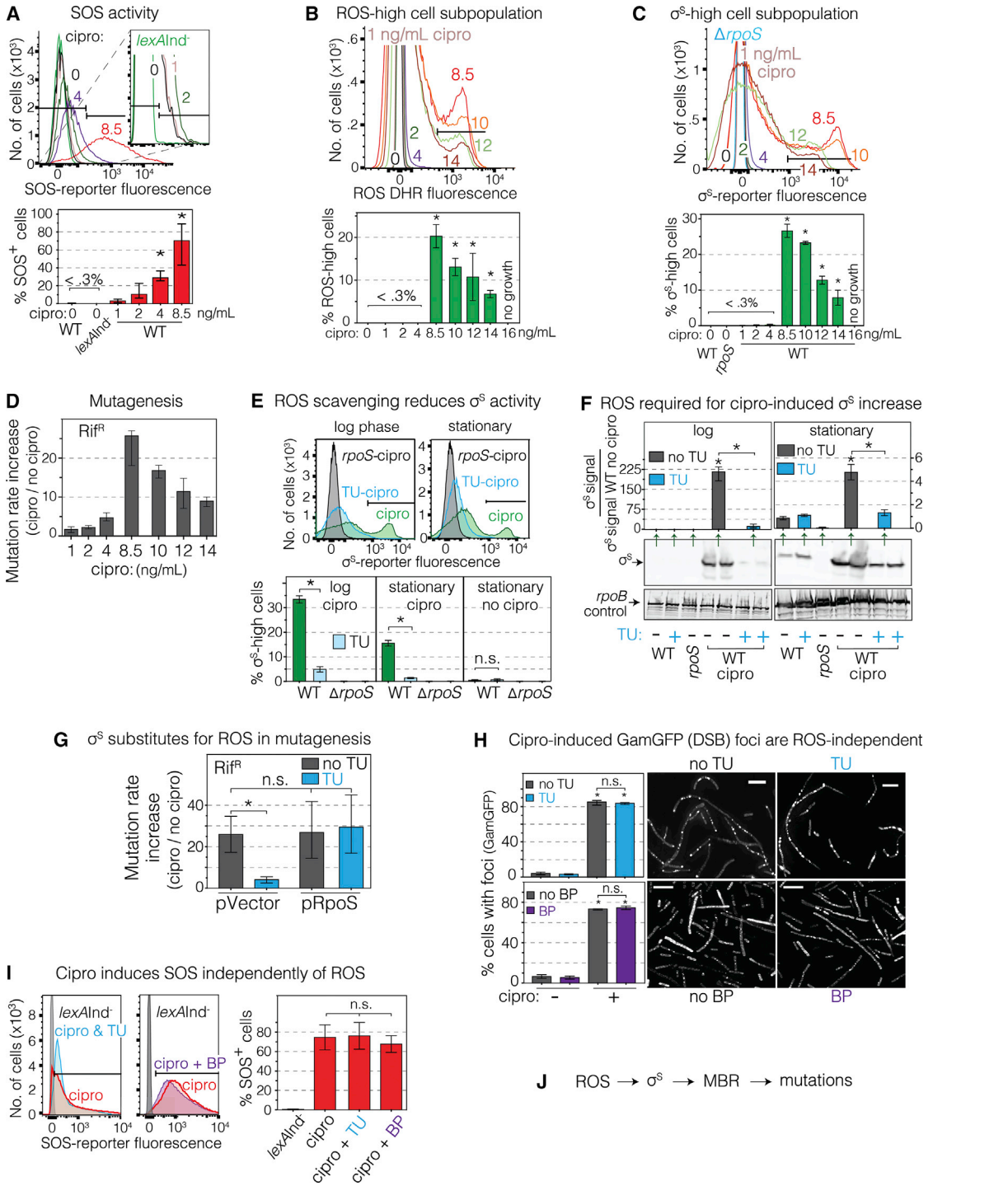

Figure 2. ROS Form in Minority Cell Subpopulation and Activate σ^S Response and MBR

(A–C) Cells analyzed in log phase growth (16 h). The MAC cipro is 8.5 ng/mL for WT. MAC doses used for all strains and shown in Table S1.

(A) Dose-dependent activation of the SOS response by cipro. Flow-cytometry with chromosomal SOS reporter P_{sulA}*mCherry*. SOS-positive cells, right of the gate shown (black bars) (STAR Methods). Afu, arbitrary fluorescence units. Means ± SEM, 3 experiments. *Different from no cipro, $p < 0.01$, one-way ANOVA with Tukey's post hoc test.

(B) MAC cipro induces high ROS in a 20% ± 3% cell subpopulation in log phase. Flow cytometry, ROS dye dihydrorhodamine 123 (DHR). ROS-high cells, within the gate (black bar). Means ± SEM, 3 experiments. *Different from no cipro, $p < 0.01$, one-way ANOVA with Tukey's post hoc test.

(legend continued on next page)

in a discreet 27% ± 3% of the cells (Figures 2C and S3B). Both ROS- or σ^S-high subpopulations arose above a threshold, with few ROS- or σ^S-high cells detected below the 8.5 ng/mL MAC dose (Figures 2B and 2C), and decreasing subpopulation sizes at higher doses (Figures 2B and 2C). This mimicks the dose response of mutagenesis (Figure 2D). MAC doses are used for all following work, e.g., (Figures 3 and 4) unless stated otherwise. ROS- and σ^S-high subpopulation sizes change throughout growth, peaking in log phase (16 h) and declining to near 10% at stationary phase (24 h, 48 h) (Figures 2E and S3C), when mutagenesis is assayed (Figure 4A, graphs; Table S3, time survey). Antibiotic growth inhibition requires ROS (Kohanski et al., 2007) and also occurred above an 8.5 ng/mL threshold (Figure S3D). The discreet ~20% subpopulation(s) of the log phase cells have very high ROS or σ^S-activity (Figures 2B and 2C).

ROS scavenging or preventing agents TU or BP blocked σ^S-response induction, as seen in loss of the σ^S-high subpopulation (Figures 2E and S3E), a reduction of accumulated σ^S-protein (Figure 2F), and as reduction of activity from a σ^S-β-galactosidase reporter (Figure S3F). Thus, ROS are required for induction of the σ^S response, as they are for mutagenesis (Figures 1D, S5A, and S5B, additional controls).

Moreover, engineered σ^S upregulation fully substituted for ROS in mutagenesis (Figures 2G, S5C, and S5D), implying that the main role of ROS in cipro-induced MBR (Figure 1D) is σ^S induction. ROS and σ^S also act in the same mutation pathway (Figure S1F). Cells with active but cipro-non-binding GyrA* and ParC* mutant proteins (Khodursky et al., 1995) showed no induction of SOS, ROS, or σ^S responses (Figures S3G–S3I), indicating that the events that lead to SOS, ROS, and σ^S induction begin with cipro interaction with its targets.

ROS promote antibiotic (growth-inhibitory) activity (Table S1) by creating DNA breaks via oxidized guanine (8-oxo-dG) in DNA (Foti et al., 2012; Kohanski et al., 2007). In contrast, reduction of cellular ROS with TU or BP, although inhibitory to the MBR mutagenesis (Figure 1D), did not reduce MAC-cipro induction of DSBs, quantified as GamGFP foci (Figures 2H and S3J), nor SOS (Figure 2I). 8-oxo-dG incorporation appears not to underlie ROS action in the mutagenesis in that ROS-mediated 8-oxo-dG-signature mutations (G-to-T and A-to-C) (Schaaper and Dunn, 1987) are less frequent in cipro-induced than spontaneous forward mutations (Figure S1C). Thus, ROS drive mutagenesis other than by promoting DNA damage, SOS, or misincorporation opposite 8-oxo-dG.

The data show that cipro action on topoisomerases leads to induction of high ROS in a discreet cell subpopulation (Figure 2B); the ROS activate σ^S in a subpopulation (Figures 2C, 2E, and 2F); and σ^S activation is how ROS promote cipro-induced MBR (Figures 2G and 2J). This constitutes a novel role for ROS in mutagenesis—signaling induction of the σ^S stress response—unlike those in antibiotic activity or starvation-stress-induced MBR (Moore et al., 2017).

σ^S-Active Gambler Cell Subpopulation Generates Mutants

Fluorescence-activated cells sorting (FACS) revealed that the small σ^S-high subpopulation produces most cipro-induced mutants (Figure 3). We sorted σ^S high- and low-activity cells in 24 h stationary cells, when 13% ± 1% of cells are σ^S- high, to at least 97% enrichment (Figures S6A–S6C). Remarkably, whereas unsorted and mock-sorted cells show (mean) 25- ± 4-fold induction of RifR mutant frequencies by cipro (Figure 3A), the sorted σ^S-high cells displayed 410- ± 70-fold induction—16 ± 3 times higher than unsorted or mock-sorted cells (Figures 3A, 3B, S6D, S6E, and S7A). Although untreated cells have higher σ^S-activity at 24 h than during log phase (4 h and 24 h) (Figure S5G), the activity is much less than in cipro-treated σ^S-high cells (Figures 4A and S5E). Moreover, the σ^S-low subpopulation, 87% ± 1% of cells, showed 8 ± 2 times fewer mutants than unsorted or mock-sorted cells (Figure 3A), indicating that few if any mutants arise in the majority subpopulation. We estimate the contribution of each subpopulation to yields of mutants as follows: because σ^S-low cells display only a 3- ± 1-fold increase in RifR mutants (Figure 3A), we can conclude that the σ^S-low cells produced ~12% of the mutants (3-fold increase/25-fold increase in unsorted/mock-sorted = 12%, Figure 3A). Thus, at least 88% of RifR mutant yield originates in the σ^S-high cells.

σ^S-high cells could have higher levels or better survival of mutagenesis. Either way, the σ^S-high cells contribute most of the mutants, and therefore most of the evolvability of the population. Death is similar in σ^S-high and -low cells (Figure S7B), suggesting that σ^S-high cells undergo more mutagenesis, rather

(C) MAC cipro induces high σ^S-response activity in a 27% ± 3% cell subpopulation in log phase. σ^S-response reporter *yiaG-yfp*. σ^S-high cells, within the gate (black bar) (STAR Methods). Note: smaller σ^S-high subpopulations of ~10% of cells in stationary phase (E below, Figures 3 and 4). Means ± range, 2 experiments. *Different from no cipro, $p < 0.01$, one-way ANOVA with Tukey's post hoc test.

(D) Cipro induction of mutagenesis occurs maximally at the 8.5 ng/mL MAC. Means ± range, ≥2 experiments.

(E) ROS are required for cipro-induced σ^S response. ROS scavenger TU removes the σ^S-high cell subpopulation in log (16 h) and stationary phase (24 h), MAC cipro. Means ± SEM, 3 experiments. *$p < 0.01$, one-way ANOVA with Tukey's post hoc test; n.s., not significant.

(F) ROS are required for MAC-cipro-induced σ^S increase. TU reduces σ^S accumulation in log (16 h) and stationary phase (24 h). Representative western blot and quantification. Means ± range, 2 experiments. *Different from no cipro, $p < 0.01$, one-way ANOVA with Tukey's post hoc test.

(G) Engineered σ^S production substitutes for ROS, allowing mutagenesis in TU-treated cells. Means ± 95% CI, ≥3 experiments. *$p < 0.01$, one-way ANOVA with Tukey's post hoc test; n.s., not significant.

(H) Cipro induces DSBs ROS independently, unaffected by TU or BP. GamGFP (DSB) foci log phase (16 h) with or without MAC cipro. Representative images. Scale bar, 5 μm. Means ± SEM, ≥3 experiments. *Different from no cipro, $p < 0.001$, one-way ANOVA with Tukey's post hoc test.

(I) SOS induction is independent of ROS, unaffected by TU or BP. Experiments as described in (A). Means ± SEM, ≥ 3 experiments, one-way ANOVA with Tukey's post hoc test; n.s., not significant.

(J) Summary: cipro-induced ROS induce the σ^S response, which allows mutagenic break repair (MBR) and mutations. Not shown: the ROS and σ^S response occur in a minority cells subpopulation(s).

See also Figures S1, S2, S3, S4, and S5 and Tables S1, S2, and S3.

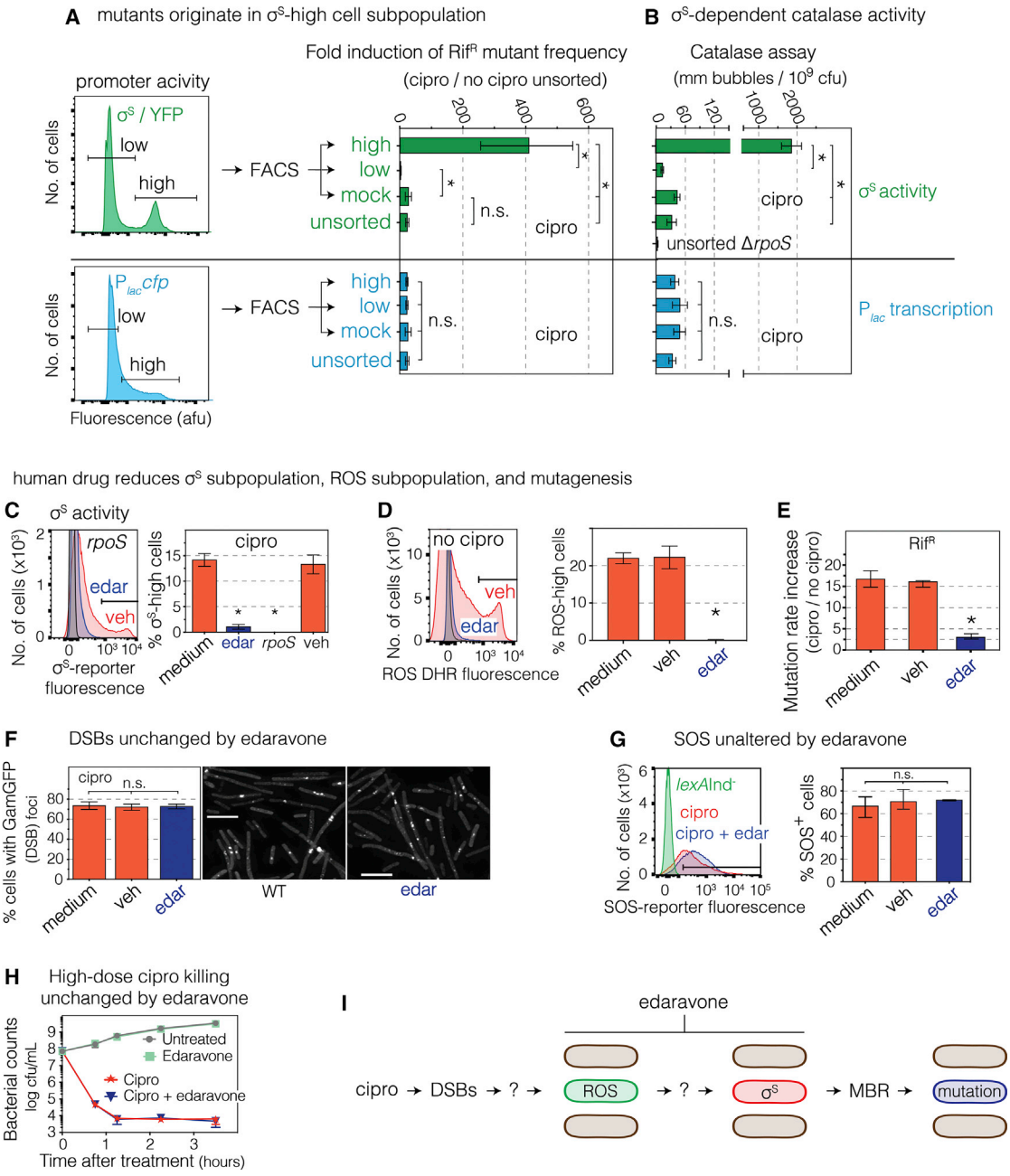

Figure 3. σ^S-Response-High Gambler Cell Subpopulation Generates Mutants and Is Inhibited by FDA-Approved Drug

(A) Most cross-resistant mutants are produced by the minority σ^S high-activity cell subpopulation. MAC cipro-treated cells (24 h) with σ^S-response or *lac* reporters FACS sorted and assayed for mutagenesis. ≥88% of cipro-induced mutants arose in 13% of cells (text). Means ± 95% CI, 3 experiments. *$p < 0.01$, one-way ANOVA with Tukey's post hoc test; n.s., not significant.

(B) High catalase activity in σ^S-high cells confirms σ^S-high status. HPII, the σ^S-regulated catalase. Means ± SEM, 3 experiments. *$p < 0.01$, one-way ANOVA with Tukey's post hoc test.

(C) FDA-approved antioxidant drug edaravone reduces the σ^S-response-activated cell subpopulation. Flow-cytometry of stationary-phase (24 h) cells. Means ± range, 2 experiments. *Different from medium, $p < 0.001$, one-way ANOVA with Tukey's post hoc test.

(D) Edaravone decreases ROS-high subpopulation as TU does (Figures 2E–2G). Flow-cytometry of log phase (16 h) cells, MAC cipro, stained with DHR ROS dye. Means ± range, 2 experiments. *Different from medium, $p < 0.001$, one-way ANOVA with Tukey's post hoc test.

(E) Edaravone inhibits cipro-induced mutagenesis. Means ± range, 2 experiments. *Different from no-drug, $p < 0.001$, one-way ANOVA with Tukey's post hoc test.

(F and G) Edaravone does not affect (F) MAC cipro induction of GamGFP (DSB) foci, log phase (16 h), scale bar 5 μm, or (G) the SOS response. Means ± range, 2 experiments, one-way ANOVA with Tukey's post hoc test; n.s., not significant.

(legend continued on next page)

than exhibiting better survival. Both high σ^S activity and mutability are transient. The RifR mutants recovered are neither σ^S-high (Figure S5F) nor heritably "mutator" (Figure S7C). Greater mutant production does not result indirectly from high fluorescence (possible high metabolic activity): see P_{lac}*cfp* (Figures 3A, S2A, S2B, and S4E).

Thus, a small, transiently differentiated σ^S-high subpopulation is transiently hypermutable and produces most cipro-induced Rif (cross)-resistant mutants, suggesting a potential "bet-hedging" developmental strategy (Norman et al., 2015; Veening et al., 2008) that may allow evolution while only some cells risk mutagenesis. We call these cells gamblers.

Food and Drug Administration-Approved Drug Inhibits Evolvability

The gambler subpopulation could be a therapeutic target for inhibition of cipro-induced mutagenesis to antibiotic resistance, cross resistance, and immune evasion. We found that the ROS-reducing drug edaravone, indicated for amyotrophic lateral sclerosis (ALS) and cerebral infarction (Watanabe et al., 2018), inhibits cipro-induced mutagenesis but not its antibiotic activity. At concentrations used clinically (100 μM) (Parikh et al., 2016), edaravone inhibited the appearance of σ^S-high cells (Figure 3C), σ^S-fusion protein (Figure S3F), ROS-high cells (Figure 3D), and most (82% ± 1% of) RifR mutagenesis (Figure 3E). Edaravone did not affect cipro induction of DSBs (Figure 3F), SOS (Figure 3G), cell growth (Figure S2A), colony formation (Figure S2B), or negative-control β-gal activity (Figure S5B), implying specific inhibition of σ^S induction (Figure 3I). Importantly, edaravone did not reduce high-dose cipro killing (Figure 3H), showing that it can reduce mutagenesis without altering cipro utility as an antibiotic. These data serve as a proof-of-concept for small-molecule inhibitors that could be administered with antibiotics to reduce resistance evolution by impeding differentiation of gamblers, without harming antibiotic activity.

ROS-High Cells Become Gamblers via Small RNAs

We explored how gamblers are differentiated (Figure 3I), following single cells over time with flow cytometry and found that ROS (DHR dye, green) appear 4 h after cipro addition, before σ^S activity (red fluorescence reporter) is detectable (Figure 4A; STAR Methods). Double-positive ROS (green) σ^S-active (red) cells develop between 8 and 16 h (Figures 4A and S5G), showing that at least some σ^S-high cells begin as ROS-high cells. At 24 h, when cells were harvested for sorting and/or mutagenesis assays (Figures 1A and 1B), many double-positive ROS- and σ^S-high cells were present (Figure 4A, upper right quadrant, 24 h), as were some σ^S-high single-positive cells (Figure 4A, lower right quadrant, 24 h). We used live-cell imaging with fluorescence-reporter genes (green) for two different oxidative stress responses, in cells that also carry the red σ^S-response reporter, to follow single live cells over time from their burst of ROS to σ^S-response induction. The reporters are transcriptional GFP fusions for *oxyR* (peroxide) and *sodA* (superoxide) responses, and both show double-positive and some σ^S-single-positive cells with flow cytometry at 24 h (Figure 4B).

Time-lapse microscopy showed that essentially all red σ^S-active gambler cells arose from oxidative-stress-response-activated green cells (*sodA* reporter, >99%) (Figure 4C; Video S1). Some of the σ^S-high cells showed reduced ROS after σ^S induction (Figure 4C; Video S1), suggesting amelioration of high ROS levels by the σ^S response.

We investigated how ROS activate the σ^S response (Figure 5). σ^S is regulated at multiple levels including upregulation by small RNAs (sRNAs) ArcZ, RprA, and DsrA, that promote σ^S translation assisted by Hfq RNA chaperone (Battesti et al., 2011). Hfq, DsrA, and ArcZ, but not RprA, are required for induction of σ^S protein (Figure 5A), differentiation of the gambler subpopulation (Figure 5B), and mutagenesis Figures 5C and 5D), with no further decrease in the double or triple mutants, implying action of Hfq and the sRNAs in the same pathway (Figures 5A–5C). Further, Hfq can be substituted by production of σ^S from a plasmid, which restored 86% ± 10% of mutagenesis to Δ*hfq* cells (Figures 5D, S2A, and S2B; Table S2), implying that Hfq promotes mutagenesis mostly or wholly by promoting σ^S induction, presumably via ArcZ and DsrA sRNAs.

Moreover, cipro induced transcription of *dsrA* and *arcZ* transcriptional *lacZ* fusions ROS dependently. The reporters showed 2.3- ± 0.3-fold and 53- ± 3-fold induction by cipro in log (16 h) and 7.4- ± 0.4-fold and 48- ± 1.3-fold induction in stationary phase (24 h) (Figure 5E), both of which were reduced by TU, BP, and edaravone (Figure 5E). Thus, cipro-induced ROS increase transcription of DsrA and ArcZ sRNAs, which, with Hfq, allow creation of the σ^S-high gambler subpopulation. The smaller stationary-phase increase of σ^S activity in the main population (Figure S5G, no cipro 4 h and 24 h) did not require these sRNAs (Figure 5B, middle histogram, compare *arcZ dsrA* with *rpoS*), suggesting that they specifically allow cipro-induction of the ROS-promoted σ^S response. Although DsrA and ArcZ are necessary for ROS upregulation of σ^S and mutagenesis (Figures 5A–5C), they may not be sufficient; ROS might promote σ^S induction via other mechanisms. The sRNAs are required for, and their levels correlate with, differentiation of ROS-high subpopulation cells into σ^S-active gamblers (Figure 5F).

One way that the σ^S response is kept "off" in unstressed cells is via RssB, which delivers σ^S to the ClpXP protease for degradation. Using a *rpoS-lacZ* reporter (Zhou and Gottesman, 2006), deletion of *rssB* increased σ^S in untreated, but not in cipro-treated cells (Figure 5A), implying that detectable RssB-mediated σ^S degradation occurs without, but not with, cipro treatment. Similarly, Δ*rssB* did not increase cipro-induced mutagenesis (Figure 5C). These data suggest that cipro induction of σ^S already includes downregulation or saturation of RssB-mediated degradation.

(H) Edaravone does not reduce high-dose cipro antibiotic killing activity. Log phase cells grown with or without 1.5 μg/mL cipro. Means ± range, 2 experiments.
(I) Summary. The σ^S high-activity cell subpopulation generates most resistant mutants: a gambler cell subpopulation. FDA-approved drug edaravone inhibits mutagenesis, reduces ROS and σ^S-high gambler subpopulations. Ovals, *E. coli* cells.
See also Figures S2, S4, S5, S6, and S7 and Tables S1 and S2.

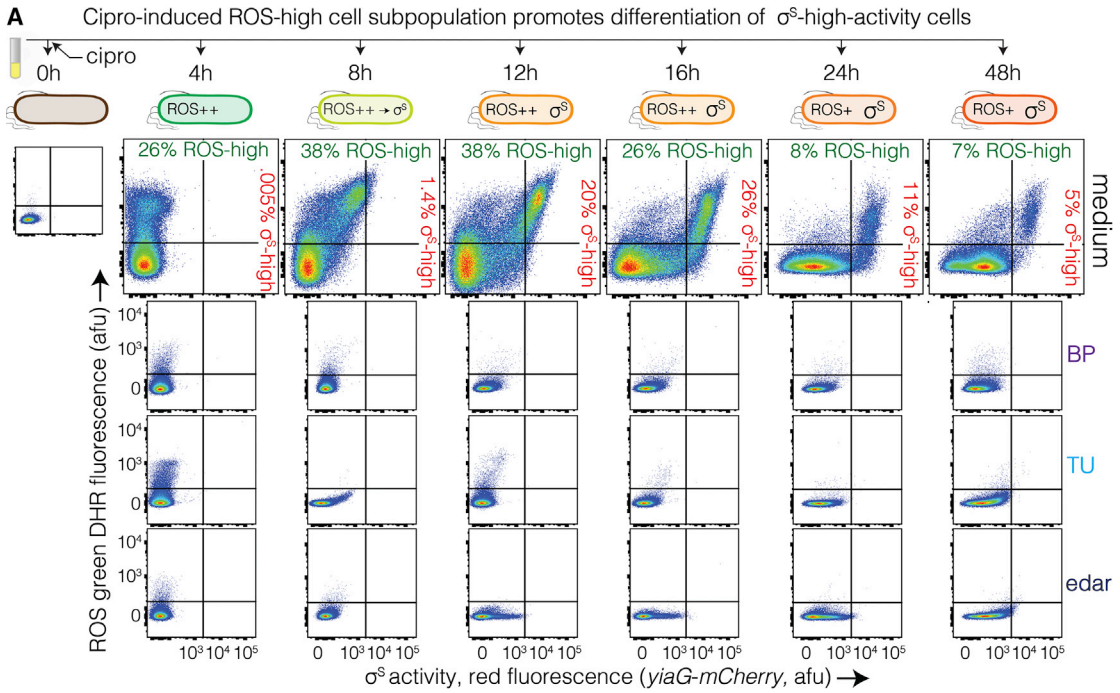

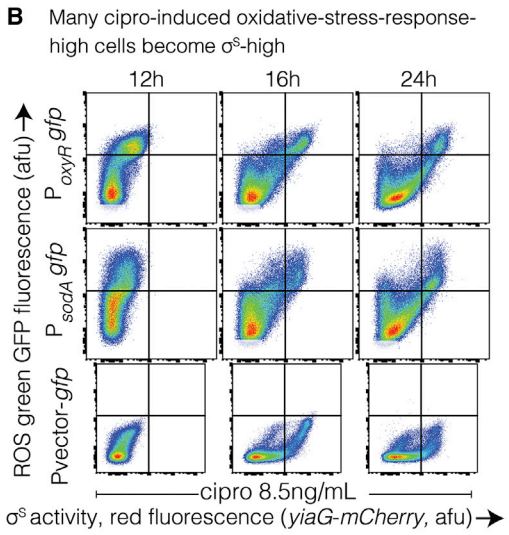

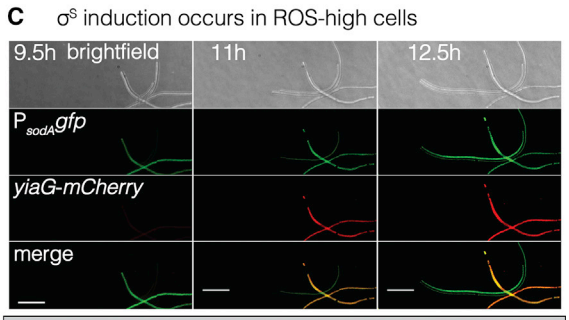

Progression of states of individual cells from 9-24h		
State at 24h	History from 9-19h	Histories of 24h σS-on (red) single cells (% of cells with each history)
σS (red)	ROS (green)	> 99.6%
σS (red)	no ROS (no signal)	< 0.4%
Fate at 24h	State from 9-19h	Fates of 9-19h ROS-high (green) single cells (% of cells with each fate)
σS (red)	ROS (green)	54% ± 9%
ROS (green)	ROS (green)	28% ± 7%
no ROS	ROS (green)	19% ± 2%

Figure 4. ROS-High Subpopulation Cells Become σS-High Cells

(A) ROS-high cells become many of the σS high cells. Flow cytometry time course of cells with MAC cipro, with and without ROS reducers BP, TU, or edaravone (edar). ROS-high cells precede σS-high cells, and double-positive cells (upper right quadrants 8–48 h) indicate that many σS-high cells arise from ROS-high cells. Representative of 3 experiments.

(B) Live ROS-high cells, detected by P_{oxyR}*gfp* or P_{sodA}*gfp* oxidative-stress-response reporters. MAC cipro time course. Double-positive cells indicate that many σS-high cells had high ROS. Representative of 2 experiments.

(C) Most or all σS-high red cells arise from oxidative response-activated green cells. Live-cell time-lapse deconvolution microscopy imaging of cells carrying P_{sodA}*gfp* and σS-response reporter *yiaG-mCherry* grown with MAC (8.5 ng/mL) cipro for 8 h, were imaged over 12 additional hours. Essentially all σS-high cells at 24 h arose from cells that were ROS-high at 9–19 h (>99%). Most (54%) but not all (28%) ROS-high cells at 19 h became σS-high at 24 h, and some 19 h ROS-high cells lose their ROS by 24 h (19%). Scale bar, 10 μm. Mean ± range, 2 experiments tracking ≥250 cells.

See also Figure S5, Table S3, and Video S1.

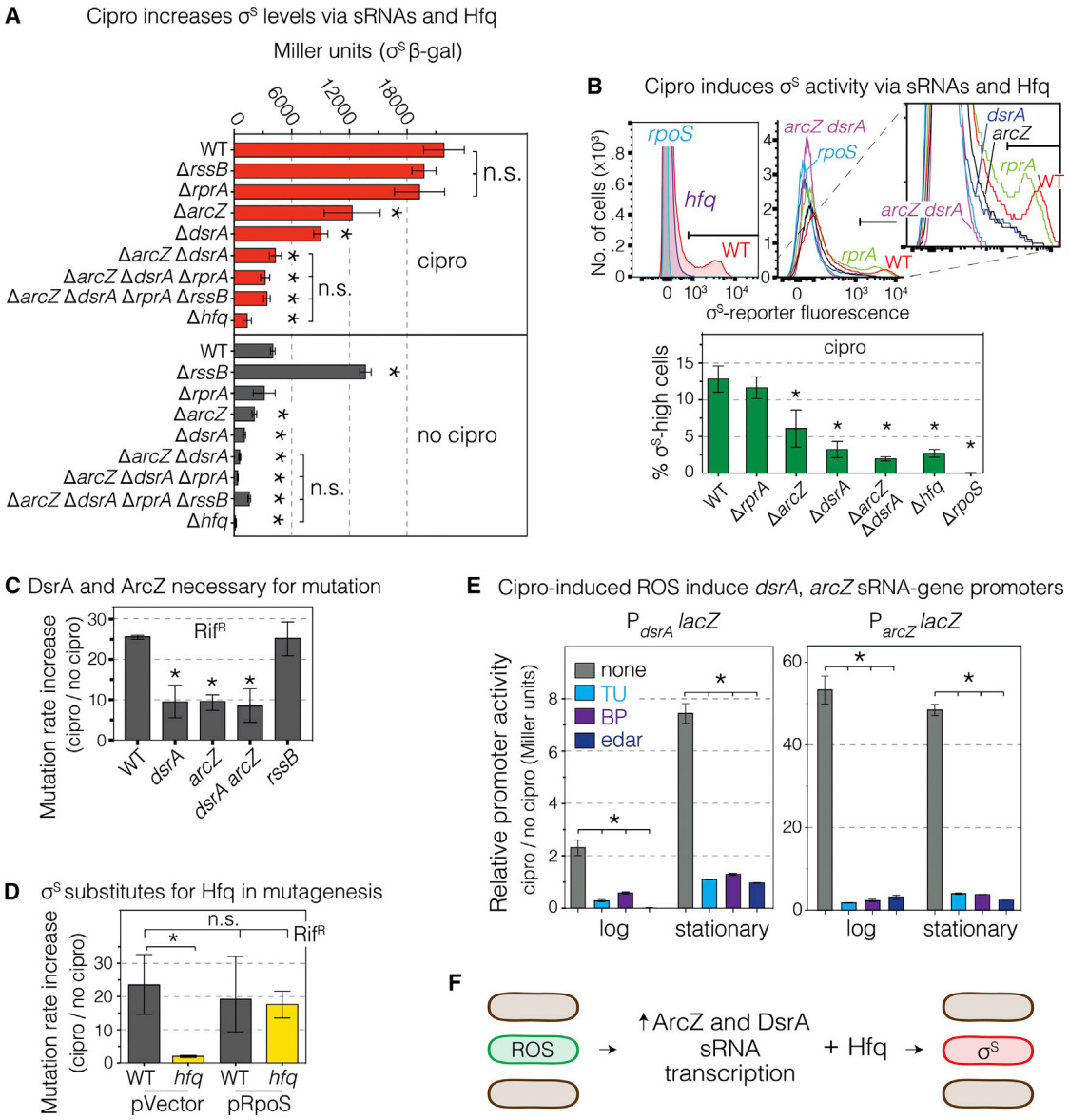

Figure 5. ROS Induce Transcription of sRNAs that Upregulate σ^S General Stress Response

(A) sRNAs DsrA and ArcZ and the Hfq RNA chaperone are required for cipro-induction of σ^S protein. Stationary phase (24 h) with MAC cipro. RssB facilitates degradation of σ^S protein. The increase of σ^S levels in Δ*rssB* cells without cipro, but not with, implies reduced σ^S degradation when cipro-induced ROS upregulate σ^S. Means ± SEM, 3 experiments. *Different from WT with cipro (top) or WT without cipro (bottom), $p < 0.01$, one-way ANOVA with Tukey's post hoc test; n.s., not significant.

(B) DsrA, ArcZ, and Hfq allow cipro induction of σ^S activity, stationary-phase (24 h). Representative flow cytometry histograms show loss of σ^S-high cells in *dsrA*, *arcZ*, and *hfq* null mutants. Means ± SEM, 3 experiments. *Different from WT, $p < 0.01$, one-way ANOVA with Tukey's post hoc test.

(C) DsrA and ArcZ required for cipro-induced mutagenesis and act in the same pathway. Means ± range, ≥2 experiments. *$p < 0.01$, one-way ANOVA with Tukey's post hoc test.

(D) Artificial upregulation of σ^S substitutes for Hfq in mutagenesis indicating that Hfq promotes mutagenesis by σ^S upregulation. Means ± 95% CI, ≥3 experiments. *Different from WT, $p < 0.01$, one-way ANOVA with Tukey's post hoc test; n.s., not significant.

(E) Cipro-induced ROS induce the *dsrA* and *arcZ* promoters. β-galactosidase activity, P_{dsrA}*lacZ*, and P_{arcZ}*lacZ* reporters in log (16 h) and stationary phase (24 h), ±ROS reducers TU, BP, or edaravone. Means ± range, 2 experiments. *Different from no drug as indicated in the figure, $p < 0.01$, one-way ANOVA with Tukey's post hoc test.

(F) Summary. Cipro-induced ROS in subpopulation cells induce transcription of DsrA and ArcZ sRNAs which, with the Hfq RNA chaperone, upregulate σ^S in the ROS-high cells (Figure 4).

See also Figures S2 and S5 and Tables S1 and S2.

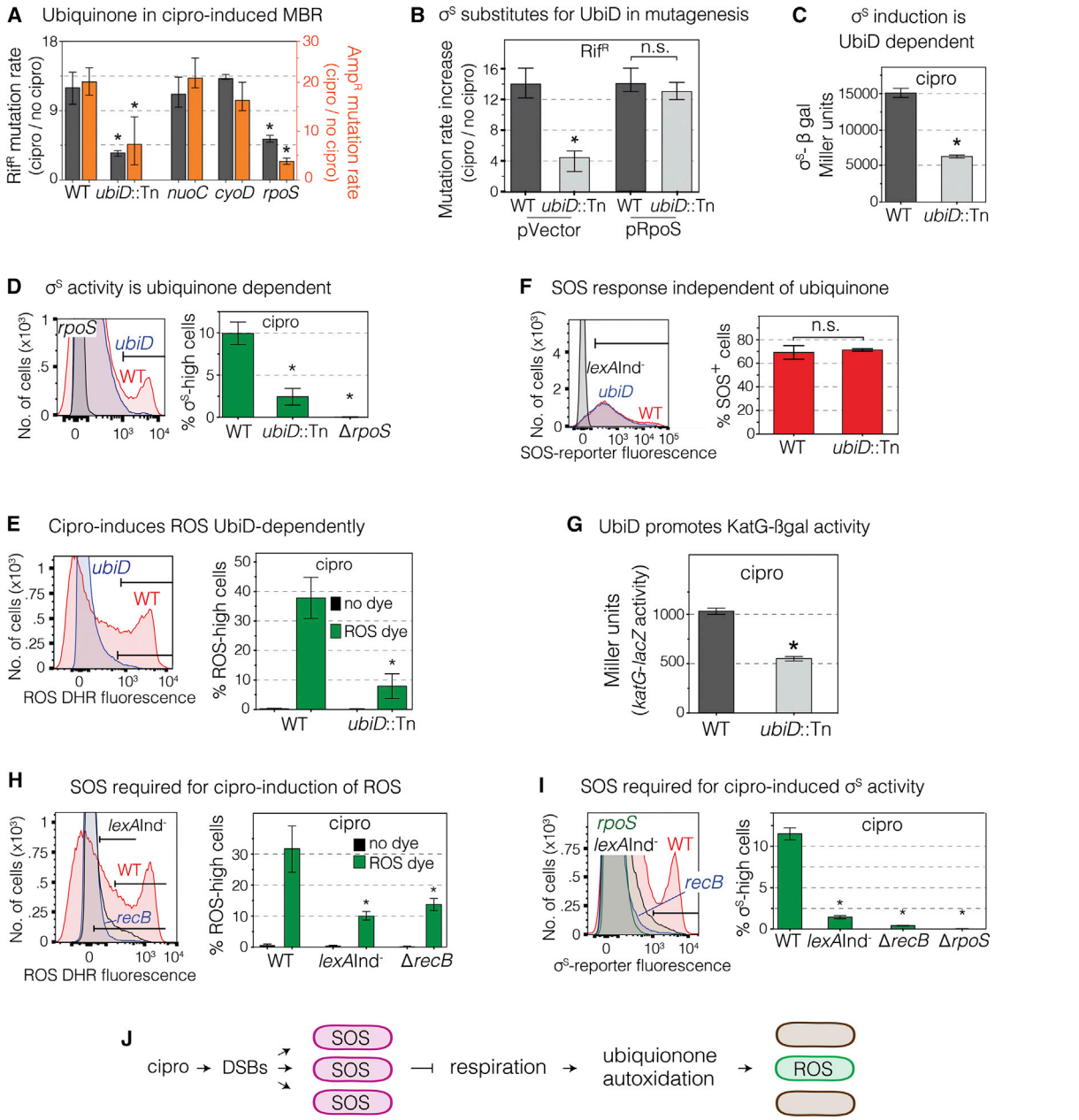

Figure 6. ROS Induction Requires SOS and Ubiquinone (Electron Transfer)

(A) Ubiquinone promotes cipro-induced mutagenesis. Mutant MACs (Table S1). Means ± CI, ≥3 experiments. *Different from WT, $p < 0.01$, one-way ANOVA with Tukey's post hoc test of natural-log transformed data.

(B) Artificial upregulation of σ^S substitutes for UbiD in mutagenesis, implying that UbiD promotes mutagenesis by upregulation of σ^S. Means ± 95% CI, ≥3 experiments. *Different from WT, $p < 0.01$, one-way ANOVA with Tukey's post hoc test of natural-log transformed data; n.s., not significant.

(C) Cipro-induced σ^S-β-galactosidase activity, reflecting σ^S accumulation, is promoted by UbiD. MAC cipro-grown 24 h stationary-phase cells. Means ± range, 2 experiments. *Different from WT, $p < 0.01$, two-tailed Student's t test.

(D) Cipro-induced σ^S activity requires UbiD. Flow-cytometry shows loss of the σ^S-high subpopulation in *ubiD*-null cells. MAC cipro-grown 24 h stationary-phase cells. Means ± SEM, 3 experiments. *Different from WT, $p < 0.01$, one-way ANOVA with Tukey's post hoc test.

(E) Cipro induction of ROS requires UbiD. ROS-positive cells in log phase (16 h) MAC cipro, seen with DHR dye. Means ± SEM, 3 experiments. *Different from WT, $p < 0.01$, one-way ANOVA with Tukey's post hoc test.

(F) Cipro induction of the SOS response does not require UbiD. SOS activity in stationary-phase (24 h) MAC cipro-grown cells. Means ± range, 2 experiments, two-tailed Student's t test; n.s. not significant.

(G) UbiD promotes cipro induction of the H_2O_2 responsive *katG-lacZ* fusion. MAC cipro log phase (16 h) cells. Means ± range, 2 experiments. *Different from WT, $p < 0.01$, two-tailed Student's t test

(legend continued on next page)

ROS Induced via SOS Response and Ubiquinone

The ROS-induction pathway is only partly characterized (Figure 3I) (Dwyer et al., 2015). We found that mutagenesis was reduced in cells lacking UbiD (biosynthesis of ubiquinone), but not other components of the electron-transfer-chain (ETC) shown to promote σ^S activity during starvation-stress-induced MBR: NuoC (ubiquinone oxidoreductase I, an ETC "complex I" subunit) and CyoD (a subunit of cytochrome bo′ oxidase, an ETC "complex II" subunit) (Al Mamun et al., 2012) (Figures 6A, S2A, and S2B). UbiD and ubiquinone appear to act upstream of σ^S-response induction in mutagenesis, in that artificial production of σ^S substituted for UbiD, restoring most or all mutagenesis (87% ± 16%) to Δ*ubiD* cells (Figure 6B). We found reduction of σ^S accumulation, σ^S activity, ROS, but not SOS activation in Δ*ubiD* (ubiquinone-deficient) cells (Figures 6C–6F), indicating that ubiquinone, and by implication, electron transfer, are required for cipro induction of the σ^S response, and act downstream of (after) SOS induction and before (upstream of and by promoting) ROS induction.

Ubiquinone functions in the aerobic ETC, mediating oxidoreduction cycles for ATP production (Meganathan and Kwon, 2009). The Δ*ubiD* cells showed severely reduced ROS in cipro with 8% ± 4% ROS-high cells in log phase compared with 32% ± 9% in wild-type (WT) (Figure 6E) and reduced *katG-lacZ* activity, a reporter activated by H_2O_2 (Figure 6G; Table S5). We can infer that SOS acts upstream of, or in parallel with, ubiquinone in ROS induction (Figure 6H), not downstream of ubiquinone, which is not needed for SOS induction (Figure 6F). In assays without cipro, SOS inhibited aerobic respiration (Swenson and Schenley, 1974) and slowed respiration-promoted autoxidation of quinols leading to superoxide (González-Flecha and Demple, 1995; Skulachev, 1998). These data without cipro, and ours with cipro, support a model in which SOS activation may inhibit the ETC leading to ROS (Figure 6J). Although necessary for the cascade to σ^S induction (Figures 6H and 6I), SOS seems not to be sufficient in that most SOS-induced cells do not display high ROS or σ^S (Figures 2A–2C). One possibility is that the cipro-induced SOS response might inhibit or slow aerobic respiration in only a cell subpopulation, allowing autoxidation of ubiquinone to produce high ROS levels preferentially in those cells (Figure 6J).

Multi-Chromosome Cells Allow Evolvability

In MAC cipro, *E. coli* forms long, multi-chromosome cell "filaments" that "bud off" small, normal-length daughter cells that produce cipro-resistant mutants efficiently (Bos et al., 2015), suggesting that multiple chromosomes might promote adaptation. Recombination or allele sharing might mitigate deleterious effects of multiple mutations (Bos et al., 2015) and/or increase repair probability allowing survival.

We reduced the multiple chromosomes and cell length by a significant half by knock-out of the SulA SOS-induced cell-division inhibitor (Figure 7), which promotes filamentation (Huisman and D'Ari, 1981). Reducing filamentation, seen by counting TetR-mCherry-marked chromosomes as foci (Figures 7A–7F) (Joshi et al., 2013), and cell size by microscopy (Figures 7D and 7E; STAR Methods, filament definition), reduced mutagenesis (Figure 7G).

Because multiple CFU in cipro might increase apparent mutation rate—mutations per CFU per generation—without increasing mutagenesis per chromosome, we counted marked chromosomes (Figure 7A) and calculated cipro-induced mutation rates per chromosome per generation. Mirroring the per-cell rates (Figure 1F), WT per-chromosome mutation rate is induced 7- ± 1.5-fold by cipro (Figure 7G; mean Amp and Rif), whereas, the per chromosome rates are not induced in mutants that lack σ^S (0.73 ± 0.03), *recA* (0.29 ± 0.11), *recB* (1.0 ± 0.19), *ruvC* (0.41 ± 0.07), Pol IV (0.64 ± 0.05), Pol II (1.0 ± 0.4), Pol V (0.83 ± 0.35), Pols II, IV, and V (0.83 ± 0.17) or are SOS-non-inducible *lexA*Ind$^-$ (1.2 ± 0.15) (Table S4, raw rates, fold inductions, p values). Δ*sulA* cells show significant reduction of per-chromosome mutation rate by cipro: 4.0- ± 0.5-fold compared with 7- ± 1.5-fold in WT (Figure 7G; Table S4), implying that mutagenesis itself is promoted by SulA/multi-chromosome cells. Per-cell mutation rate in *ruvC* cells is not reduced further by Δ*sulA* (Figure 7G; Table S4), implying that SulA promotes RuvC-dependent MBR.

We also allowed cipro-treated cells to resolve their filaments to small cells by 4–6 h growth without cipro after their 18–19 h in cipro, and mutation rate per cell per generation did not differ from the standard 24 h cipro assay (Figure S7D). Thus, neither filamentation nor mutation rate calculation method alters conclusions drawn here. Previously, SulA was required for approximately half of starvation stress-induced MBR (McKenzie et al., 2000), although whether the starving (not dividing) cells filamented was not examined, making interpretations tentative.

SulA is required for formation of the ROS-high and most of the σ^S-high gambler cells (Figures S7E and S7F) and not via promoting HR, shown with HR-defective, SOS-proficient Δ*ruvC* cells (Figure S7G). Overproduction of σ^S appeared not to substitute for SulA (Figure S7H), indicating a possible SulA role in MBR in addition to promoting σ^S. Alternatively, the optimal intensity of σ^S-high cells for mutagenesis is not known, and the profile of σ^S activity levels produced by overproduction (Figure S5D) might be altered by Δ*sulA* and insufficient for MBR in Δ*sulA* cells. SOS, which is fully required for ROS/σ^S-active gambler formation

(H) The SOS response is required for cipro induction of the ROS-high cell subpopulation. SOS non-inducible *lexA*Ind$^-$ and *recB* cells, which are defective in SOS induction by DSBs. Cells grown in low-dose MAC cipro and assayed in log phase (16 h). Means ± range of 2 independent experiments. *Different from WT at $p < 0.01$, one-way ANOVA with Tukey's post hoc test.

(I) The SOS response is required for cipro induction of the σ^S-high subpopulation. SOS non-inducible *lexA*Ind$^-$ cells and *recB* cells at 24 h MAC cipro (stationary phase). Means ± range, 2 experiments. *Different from WT, $p < 0.01$, one-way ANOVA with Tukey's post hoc test.

(J) Model for cipro-induction of ROS via the SOS response and ubiquinone. Cipro-induced DSBs activate the SOS response in all cells. SOS slows aerobic respiration (Swenson and Schenley, 1974), which promotes autoxidation of ubiquinone (González-Flecha and Demple, 1995; Skulachev, 1998), which we suggest occurs in a cell subpopulation that becomes the σ^S-high subpopulation (Figure 5).

See also Figure S4 and Tables S1 and S2.

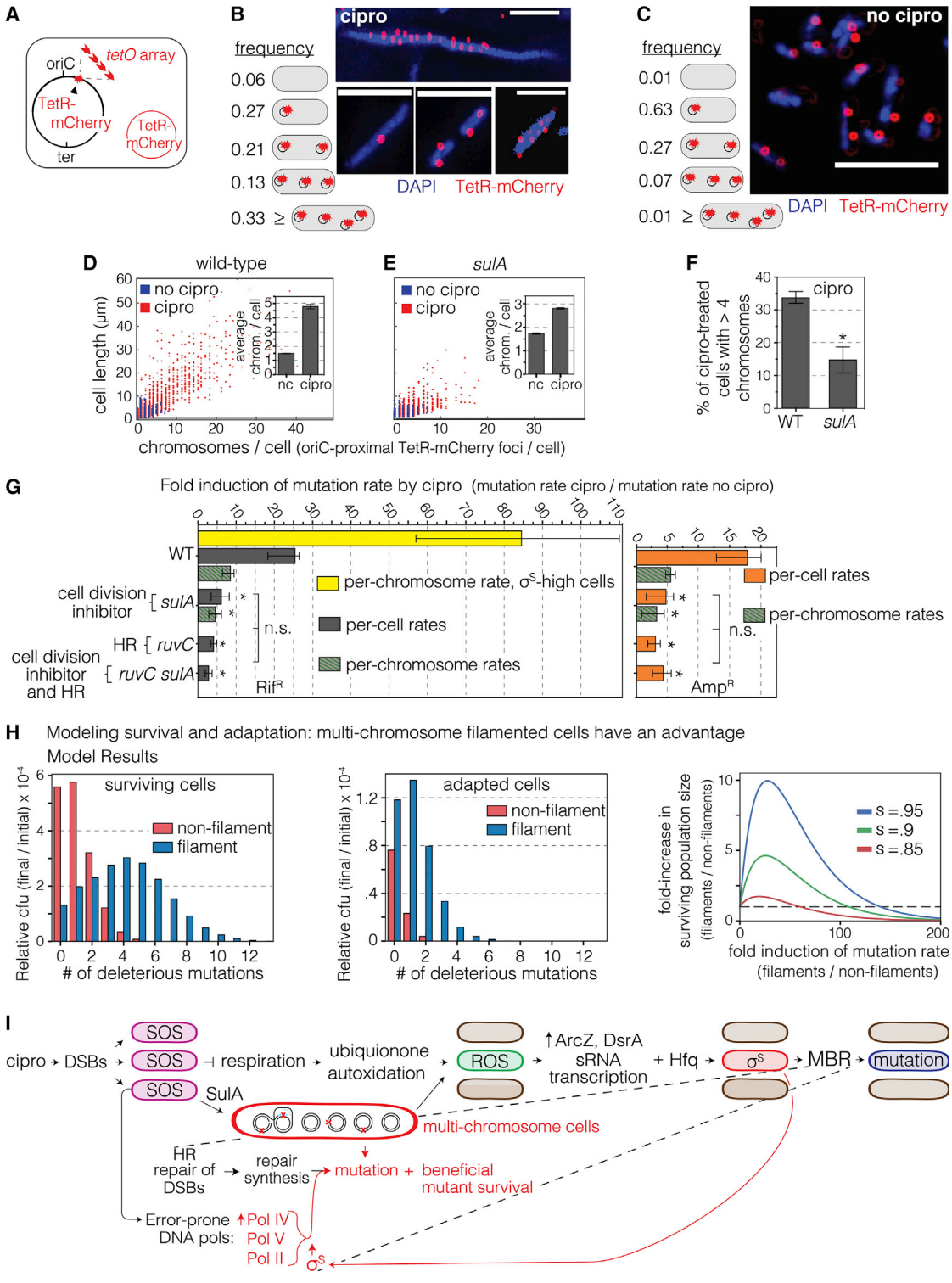

Figure 7. Multi-chromosome Bacterial Cells Promote Cipro-Induced Mutagenesis

(A) Scheme for labeling chromosomes as red fluorescent foci using a chromosomal *tetO* array bound by Tet-repressor-mCherry (TetR-mCherry) in a replication-origin (*oriC*)-proximal site. Red circle, plasmid that produces TetR-mCherry. Multiple TetR-mCherry foci represent approximate number of *ori*-proximal chromosomal equivalents (Joshi et al., 2013).

(B) More than 33% of log phase MAC cipro-grown cells carry multiple chromosomes: ≥4 per cell, detected as illustrated (A). 1,919 cells counted. Representative images of DAPI-stained WT cells. Scale bar, 5 μm.

(legend continued on next page)

(Figure 6I), appears to promote ROS/σ^S activity both SulA-dependently and SulA-independently.

We formulated a mathematical model to test possible benefits of multi-chromosome filaments for rapid adaptation (STAR Methods) per Bos et al. (2015). Results of the model (Figure 7H) show that increasing filament mutation rate increases the probability of both adaptation and survival of a chromosome relative to non-filamented cells, supporting cooperation accelerating complex adaptations (Obolski et al., 2018). The advantage of multiple chromosomes increases with increasing selection coefficient (Figure 7H) (e.g., lethality of a drug in cells under selection for resistance). This model shows that multiple chromosomes could facilitate adaptation by mutagenesis (Figure 7I, model).

DISCUSSION

Our findings (Figure 7I) unite quinolone-induced mutagenesis with σ^S-dependent stress-induced mutagenesis, defined as mutation-producing mechanisms upregulated by stress responses (Fitzgerald et al., 2017). Coupling mutagenesis to stress responses generates mutants preferentially when cells or organisms are maladapted to their environments—when stressed—potentially accelerating adaptation (Fitzgerald et al., 2017; Ram and Hadany, 2012).

ROS Regulate Mutagenesis

We found a novel regulatory and differentiating mutagenic role of ROS (Figure 7I). ROS can promote mutagenesis by direct mechanisms, including oxidation of guanines to 8-oxo-dG, which pairs with A, causing G-to-T and T-to-G (A-to-C) mutations (Schaaper and Dunn, 1987). Also, the repair of 8-oxo-dG in DNA causes DSBs (Foti et al., 2012). Neither the mutation signature of 8-oxo-dG nor ROS-dependent DNA break formation is observed (Figures 2H, S1B, and S1C), counter-indicating both possible mechanisms. Rather, the ROS mutagenic role can be substituted by production of σ^S, which activates the general (also known as starvation) stress response (Figure 2G) and allows MBR, showing that σ^S activation is the main role of ROS in the mutagenesis. The ROS induce transcription of ArcZ and DsrA sRNAs (Figure 5E), which, assisted by Hfq RNA chaperone (Figures 5A–5F), promote translation of σ^S protein (Battesti et al., 2011), which allows MBR mutagenesis (Figures 1E–1I, 3A, and 7I). This differs from a mutagenic role of Hfq with another sRNA via downregulation of translation of a mismatch-repair protein (Chen and Gottesman, 2017). Induction of ROS by cipro precedes σ^S-response activation (Figure 4), and the ROS-high cells become σ^S-high cells (Figure 4C; Video S1) that generate mutants (Figure 3A). These data highlight the centrality of stress-response-control of mutagenesis and show that ROS are signaling molecules in this regulation.

Mutagenesis in Transiently Differentiated Gamblers

Cipro-induced ROS lead to high σ^S activity in a 10%–25% cell subpopulation (Figures 2B, 2C, 2E, and 4) that is transiently mutable (Figure S7B) and produces most of the mutants (Figures 3A and 3C). Transient differentiation in subpopulations is a potential evolutionary "bet-hedging" strategy, in which some cells risk a phenotype that may be advantageous, or not, depending on the environment (Norman et al., 2015; Veening et al., 2008). "Persisters" tolerate lethal drugs but reduce proliferation (Balaban et al., 2004). Competence for natural transformation (Chen and Dubnau, 2004), sporulation (Norman et al., 2015), and even programmed cell death (Amitai et al., 2009; González-Pastor et al., 2003) are hypothesized or demonstrated (González-Pastor et al., 2003) to aid siblings of the sacrificed bacteria. Limitation of mutagenesis to a subpopulation appears to embed environmentally tuned mutagenesis within a "bet hedging" strategy (Norman et al., 2015; Torkelson et al., 1997; Veening

(C) Fewer than 1% of log phase cells grown without cipro have $\geq$4 chromosomes per cell, detected as illustrated (A). 3,915 cells counted. Representative images. Scale bar, 5 μm.

(D–F) Cipro induction of the multi-chromosome state requires SulA. Scatterplots of microscopically determined distributions of cell lengths (μm) and chromosome (TetR-mCherry) foci with and without MAC cipro. Data from 3 experiments.

(D) Cipro induction of multi-chromosome cells.

(E) SulA is required for the cipro-induction of long, multi-chromosome cells. 98% of untreated cells show $\leq$4 chromosomes per cell, more than half dependent on SulA. nc, no cipro. Means ± SEM, 3 experiments. *Different from WT at $p < 0.001$, one-way ANOVA with Tukey's post-hoc test.

(F) Δ*sulA* reduces Cipro induction of cells with >4 chromosomes. Means ± SEM, 3 experiments. *Different from WT at $p < 0.001$, two-tailed Student's t test.

(G) The SulA-dependent multi-chromosome state promotes cipro-induced mutagenesis. SulA and RuvC act in the same MBR pathway (are epistatic). Data also presented as fold induction of mutation rate per chromosome per generation (green bars). *sulA* cells still show less mutagenesis than WT ($p < 0.05$). The induction of mutagenesis in σ^S-high cells per chromosome per generation (yellow bar) exceeds unsorted WT using either mutations per chromosome or per cell per generation ($p < 0.01$). Means ± 95% CI, $\geq$4 experiments. *Different from WT, $p < 0.05$, one-way ANOVA with Tukey's post hoc test of natural-log transformed data; n.s., not significant.

(H) Mathematical model shows that multi-chromosome filaments have a large advantage for adaptation and survival at high mutation rates. Left: expected relative CFU of all surviving cells (adapted and not-adapted) as a function of the number of deleterious mutations accumulated. Middle: the expected relative CFU of adapted cells as function of the number of deleterious mutations accumulated. Right: formation of multi-chromosome filaments can increase the surviving population size when selection is harsh. We plot the fold-increase of surviving population size due to filamentation as function of the fold increase in mutation rate due to filamentation, for several selection parameters. s, selection coefficient of the major stress (e.g., antibiotics). Model description and parameters: STAR Methods.

(I) Model: mechanism of cipro-induced transient differentiation of an evolvable gambler cell subpopulation that allows stress-responsive MBR without risk to most cells. Left to right: cipro-binding to type II topoisomerases causes DSBs that activate the SOS response throughout the cell population. SOS upregulates error-prone DNA polymerases and SulA, which inhibits cell division causing multi-chromosome cells. We suggest that SOS also slows aerobic respiration in a cell subpopulation, which generates ROS subpopulation cells promoted by autoxidation of ETC component ubiquinone. The ROS activate transcription of σ^S-upregulating sRNAs DsrA and ArcZ, which, with Hfq RNA chaperone, promote translation of σ^S protein, thus activating the general stress response in the cell subpopulation, and allowing MBR in those cells—a transient hypermutable state in gambler cells (red cells). The multi-chromosome state promotes survival and adaptation of highly mutated cells by amelioration (complementation and reassortment) of deleterious recessive mutant phenotypes generated.

See also Figures S2, S3, S4, and S7 and Tables S1, S2, and S4.

et al., 2008). Although transiently mutable subpopulations have been hypothesized (Hall, 1990; Ninio, 1991), supported by genetic evidence (Torkelson et al., 1997), and cells with stress responses have been linked to mutagenesis of unknown mechanism (Woo et al., 2018), our data provide the first isolation (Figure 3) of a hypermutable cell subpopulation in the act of mutagenesis and show the defining, differentiating inputs: ROS and the general stress response (Figures 3 and 4). Our data also reveal the mutagenesis mechanism in the subpopulation: MBR (Figure 7I). These are novel mechanisms of potential promotion of the ability to evolve. Unlike "persisters," these cells take the risk of inducing mutations, which can lead to heritable resistance to never-before-encountered antibiotics. They are "gamblers."

Drugging Evolvability

The Food and Drug Administration (FDA)-approved drug edaravone behaved as an "anti-evolvability" drug by removing the ROS- then σ^S-high gambler subpopulation, without reducing the antibiotic power of cipro (Figures 3C–3I), providing a promising proof-of-concept. Other ROS-promoted mutagenesis mechanisms may involve upregulation of the σ^S response and therefore be similarly susceptible. σ^S promotes MBR (Lombardo et al., 2004; Ponder et al., 2005; Shee et al., 2011), downregulates mismatch repair activity (Gutierrez et al., 2013) and activates transposition (Ilves et al., 2001) and possibly other mechanisms. Stress-response regulators, such as σ^S, are nonredundant hubs in the MBR network (Al Mamun et al., 2012), making them attractive targets for drugs to slow evolution of pathogen resistance and immune evasion (Al Mamun et al., 2012; Fitzgerald et al., 2017; Rosenberg and Queitsch, 2014).

Multi-Chromosome Cells Promote Evolvability

Multiple chromosomes may aid mutagenesis by providing more repair partners for MBR and/or promoting adaptation by cooperation (Obolski et al., 2018). Cooperation may include the sharing of alleles (recombination) and/or gene products (while compensatory mutations occur), which could mask deleterious phenotypes (Figures 7H and 7I) allowing survival before optimized genotypes arise. Cell "filaments" may be biomarkers of rapid evolution. *Bacillus subtilis* undergoes natural transformation activated by the Com stress response, which also upregulates mutagenesis (Sung and Yasbin, 2002), thus engaging recombination with mutagenesis (Lenhart et al., 2012). *E. coli* is incapable of natural transformation but may achieve the mutate-and-recombine (or share) strategy via multiple sibling chromosomes within one cell, rather than exogenous sibling DNA. In addition to targeting stress-response regulators as an anti-evolvability drug strategy (Al Mamun et al., 2012; Fitzgerald et al., 2017; Rosenberg and Queitsch, 2014) (Figures 3C–3H), dividing (and conquering) the multiple chromosomes might also reduce evolvability as a therapeutic strategy.

STAR★METHODS

Detailed methods are provided in the online version of this paper and include the following:

- KEY RESOURCES TABLE
- CONTACT FOR REAGENTS AND RESOURCE SHARING
- EXPERIMENTAL MODEL AND SUBJECT DETAILS
- METHOD DETAILS
  - Strains, Media, and Growth
  - Bacterial Strains Used in Each Figure
  - Assays for Ciprofloxacin-induced Mutagenesis
  - Reconstruction Experiments
  - Competition Experiments
  - Flow Cytometric Assays for σ^S- and SOS-Response-Regulated Promoter Activity
  - Fluorescence-Activated Cell Sorting
  - HPII Catalase Activity
  - Microscopy and Quantification of GamGFP (DSB) and TetR-mCherry (Chromosome) Foci
  - Live Cell Deconvolution Microscopy
  - *rpoB* and *ampD* Sequencing
  - Western Analyses of σ^S Protein Levels
  - Beta-galactosidase Assays
  - Flow Cytometric Detection of Intracellular ROS or GFP and σ^S Activity in Single Cells
  - Controls for Appearance of ROS-high Subpopulation Before σ^S-high Subpopulation
  - Experimental Definition of Cipro-induced Multi-chromosome Cell Filaments
  - Mathematical Modeling of Cipro-induced Multi-chromosome Cell Filaments
  - Measurement of High-Dose Cipro Antibiotic Activity
  - Nalidixic-Acid Test for Heritable Hypermutability
  - Flow-Cytometric Detection of Dead Cells
  - Statistics

SUPPLEMENTAL INFORMATION

Supplemental Information can be found online at https://doi.org/10.1016/j.molcel.2019.02.037.

ACKNOWLEDGMENTS

We thank S. Gottesman, J. Imlay, I. Matic, and L. Zechiedrich for *E. coli* strains, N. Majdalani and S. Kozmin for advice, S. Henikoff for helpful conversation, K.M. Miller and Meng Wang for improving the manuscript, and appreciate the expert assistance of J.M. Sederstrom. This work was supported by NIH (R35-GM122598 to S.M.R., R01-GM088653 to C.H., R01-GM102679 to D.B., and R01-GM106373 to P.J.H.), the Israeli Science Fund (ISF 1568/13 to L.H.), Baylor College of Medicine (BCM) Integrated Microscopy Core funded by NIH (DK56338 and CA125123) and the Dan L. Duncan Comprehensive Cancer Center, postdoctoral fellowships from the Cancer Prevention and Research Institute of Texas BCM Cancer Training Program, and the American Cancer Society (RP160283 and 132206-PF-18-035-01-DMC to D.M.F.), the John S. Dunn Gulf Coast Consortium for Chemical Genomics, and the BCM Cytometry and Cell Sorting Core (NIH P30 AI036211, P30 CA125123, and S10 RR024574).

AUTHOR CONTRIBUTIONS

J.P.P., L.G.-V., O.L.-E., J.B., R.H.A., C.H., L.H., and S.M.R. conceived the project and advanced hypotheses and/or designed experiments. J.P.P., L.G.-V., Y.Z., A.W., J.L., J.X., and Q.M. performed or guided the work. D.M.F. and D.B. provided advice and/or assistance. J.P.P., P.J.H., and S.M.R. wrote the manuscript.

DECLARATION OF INTERESTS

The authors declare no competing interests.

Received: September 11, 2018
Revised: January 17, 2019
Accepted: February 26, 2019
Published: April 1, 2019

SUPPORTING CITATIONS

The following references appear in the Supplemental Information: Frenoy and Bonhoeffer (2018).

REFERENCES

Al Mamun, A.A.M., Lombardo, M.-J., Shee, C., Lisewski, A.M., Gonzalez, C., Lin, D., Nehring, R.B., Saint-Ruf, C., Gibson, J.L., Frisch, R.L., et al. (2012). Identity and function of a large gene network underlying mutagenic repair of DNA breaks. Science *338*, 1344–1348.

Amitai, S., Kolodkin-Gal, I., Hananya-Meltabashi, M., Sacher, A., and Engelberg-Kulka, H. (2009). *Escherichia coli* MazF leads to the simultaneous selective synthesis of both "death proteins" and "survival proteins". PLoS Genet. *5*, e1000390.

Balaban, N.Q., Merrin, J., Chait, R., Kowalik, L., and Leibler, S. (2004). Bacterial persistence as a phenotypic switch. Science *305*, 1622–1625.

Battesti, A., Majdalani, N., and Gottesman, S. (2011). The RpoS-mediated general stress response in *Escherichia coli*. Annu. Rev. Microbiol. *65*, 189–213.

Bos, J., Zhang, Q., Vyawahare, S., Rogers, E., Rosenberg, S.M., and Austin, R.H. (2015). Emergence of antibiotic resistance from multinucleated bacterial filaments. Proc. Natl. Acad. Sci. USA *112*, 178–183.

Chen, I., and Dubnau, D. (2004). DNA uptake during bacterial transformation. Nat. Rev. Microbiol. *2*, 241–249.

Chen, J., and Gottesman, S. (2017). Hfq links translation repression to stress-induced mutagenesis in *E. coli*. Genes Dev. *31*, 1382–1395.

Cirz, R.T., Chin, J.K., Andes, D.R., de Crécy-Lagard, V., Craig, W.A., and Romesberg, F.E. (2005). Inhibition of mutation and combating the evolution of antibiotic resistance. PLoS Biol. *3*, e176.

Cowen, L.E., and Lindquist, S. (2005). Hsp90 potentiates the rapid evolution of new traits: drug resistance in diverse fungi. Science *309*, 2185–2189.

Drlica, K. (1999). Mechanism of fluoroquinolone action. Curr. Opin. Microbiol. *2*, 504–508.

Dwyer, D.J., Collins, J.J., and Walker, G.C. (2015). Unraveling the physiological complexities of antibiotic lethality. Annu. Rev. Pharmacol. Toxicol. *55*, 313–332.

Fitzgerald, D.M., Hastings, P.J., and Rosenberg, S.M. (2017). Stress-induced mutagenesis: implications in cancer and drug resistance. Annu. Rev. Cancer Biol. *1*, 119–140.

Foti, J.J., Devadoss, B., Winkler, J.A., Collins, J.J., and Walker, G.C. (2012). Oxidation of the guanine nucleotide pool underlies cell death by bactericidal antibiotics. Science *336*, 315–319.

Frenoy, A., and Bonhoeffer, S. (2018). Death and population dynamics affect mutation rate estimates and evolvability under stress in bacteria. PLoS Biol. *16*, e2005056.

Gibson, J.L., Lombardo, M.-J., Thornton, P.C., Hu, K.H., Galhardo, R.S., Beadle, B., Habib, A., Magner, D.B., Frost, L.S., Herman, C., et al. (2010). The sigma(E) stress response is required for stress-induced mutation and amplification in *Escherichia coli*. Mol. Microbiol. *77*, 415–430.

González-Flecha, B., and Demple, B. (1995). Metabolic sources of hydrogen peroxide in aerobically growing *Escherichia coli*. J. Biol. Chem. *270*, 13681–13687.

González-Pastor, J.E., Hobbs, E.C., and Losick, R. (2003). Cannibalism by sporulating bacteria. Science *301*, 510–513.

Gutierrez, A., Laureti, L., Crussard, S., Abida, H., Rodríguez-Rojas, A., Blázquez, J., Baharoglu, Z., Mazel, D., Darfeuille, F., Vogel, J., and Matic, I. (2013). β-Lactam antibiotics promote bacterial mutagenesis via an RpoS-mediated reduction in replication fidelity. Nat. Commun. *4*, 1610.

Hadany, L., and Beker, T. (2003a). Fitness-associated recombination on rugged adaptive landscapes. J. Evol. Biol. *16*, 862–870.

Hadany, L., and Beker, T. (2003b). On the evolutionary advantage of fitness-associated recombination. Genetics *165*, 2167–2179.

Hall, B.G. (1990). Spontaneous point mutations that occur more often when advantageous than when neutral. Genetics *126*, 5–16.

Hall, B.M., Ca, C.X., Liang, P., and Singh, K.K. (2009). Fluctuation analysis CalculatOR: a web tool for the determination of mutation rate using Luria-Delbruck fluctuation analysis. Bioinformatics *25*, 1564–1565.

Huisman, O., and D'Ari, R. (1981). An inducible DNA replication-cell division coupling mechanism in *E. coli*. Nature *290*, 797–799.

Ilves, H., Hõrak, R., and Kivisaar, M. (2001). Involvement of sigma(S) in starvation-induced transposition of *Pseudomonas putida* transposon Tn4652. J. Bacteriol. *183*, 5445–5448.

Iwase, T., Tajima, A., Sugimoto, S., Okuda, K., Hironaka, I., Kamata, Y., Takada, K., and Mizunoe, Y. (2013). A simple assay for measuring catalase activity: a visual approach. Sci. Rep. *3*, 3081.

Joshi, M.C., Magnan, D., Montminy, T.P., Lies, M., Stepankiw, N., and Bates, D. (2013). Regulation of sister chromosome cohesion by the replication fork tracking protein SeqA. PLoS Genet. *9*, e1003673.

Khodursky, A.B., Zechiedrich, E.L., and Cozzarelli, N.R. (1995). Topoisomerase IV is a target of quinolones in *Escherichia coli*. Proc. Natl. Acad. Sci. USA *92*, 11801–11805.

Kohanski, M.A., Dwyer, D.J., Hayete, B., Lawrence, C.A., and Collins, J.J. (2007). A common mechanism of cellular death induced by bactericidal antibiotics. Cell *130*, 797–810.

Kohanski, M.A., DePristo, M.A., and Collins, J.J. (2010). Sublethal antibiotic treatment leads to multidrug resistance via radical-induced mutagenesis. Mol. Cell *37*, 311–320.

Kuzminov, A. (1999). Recombinational repair of DNA damage in *Escherichia coli* and bacteriophage lambda. Microbiol. Mol. Biol. Rev. *63*, 751–813.

Lenhart, J.S., Schroeder, J.W., Walsh, B.W., and Simmons, L.A. (2012). DNA repair and genome maintenance in *Bacillus subtilis*. Microbiol. Mol. Biol. Rev. *76*, 530–564.

Lombardo, M.-J., Aponyi, I., and Rosenberg, S.M. (2004). General stress response regulator RpoS in adaptive mutation and amplification in *Escherichia coli*. Genetics *166*, 669–680.

Lorian, V., and De Freitas, C.C. (1979). Minimal antibiotic concentrations of aminoglycosides and beta-lactam antibiotics for some gram-negative bacilli and gram-positive cocci. J. Infect. Dis. *139*, 599–603.

Magrini, E.T.N. (2017). Global priority list of antibiotic-resistant bacteria to guide research, discovery, and development of new antibiotics. Essential medicines and health products (World Health Organization), pp. 1–7.

McKenzie, G.J., Harris, R.S., Lee, P.L., and Rosenberg, S.M. (2000). The SOS response regulates adaptive mutation. Proc. Natl. Acad. Sci. USA *97*, 6646–6651.

Meganathan, R., and Kwon, O. (2009). Biosynthesis of Menaquinone (Vitamin K2) and Ubiquinone (Coenzyme Q). Ecosal Plus *3*, https://doi.org/10.1128/ecosalplus.3.6.3.3.

Moore, J.M., Correa, R., Rosenberg, S.M., and Hastings, P.J. (2017). Persistent damaged bases in DNA allow mutagenic break repair in *Escherichia coli*. PLoS Genet. *13*, e1006733.

Nehring, R.B., Gu, F., Lin, H.Y., Gibson, J.L., Blythe, M.J., Wilson, R., Bravo Núñez, M.A., Hastings, P.J., Louis, E.J., Frisch, R.L., et al. (2016). An ultra-dense library resource for rapid deconvolution of mutations that cause phenotypes in *Escherichia coli*. Nucleic Acids Res. *44*, e41.

Ninio, J. (1991). Transient mutators: a semiquantitative analysis of the influence of translation and transcription errors on mutation rates. Genetics *129*, 957–962.

Norman, T.M., Lord, N.D., Paulsson, J., and Losick, R. (2015). Stochastic switching of cell fate in microbes. Annu. Rev. Microbiol. *69*, 381–403.

Obolski, U., Ram, Y., and Hadany, L. (2018). Key issues review: evolution on rugged adaptive landscapes. Rep. Prog. Phys. *81*, 012602.

Parikh, A., Kathawala, K., Tan, C.C., Garg, S., and Zhou, X.F. (2016). Development of a novel oral delivery system of edaravone for enhancing bioavailability. Int. J. Pharm. *515*, 490–500.

Pennington, J.M., and Rosenberg, S.M. (2007). Spontaneous DNA breakage in single living *Escherichia coli* cells. Nat. Genet. *39*, 797–802.

Petrosino, J.F., Pendleton, A.R., Weiner, J.H., and Rosenberg, S.M. (2002). Chromosomal system for studying AmpC-mediated beta-lactam resistance mutation in *Escherichia coli*. Antimicrob. Agents Chemother. *46*, 1535–1539.

Ponder, R.G., Fonville, N.C., and Rosenberg, S.M. (2005). A switch from high-fidelity to error-prone DNA double-strand break repair underlies stress-induced mutation. Mol. Cell *19*, 791–804.

Ram, Y., and Hadany, L. (2012). The evolution of stress-induced hypermutation in asexual populations. Evolution *66*, 2315–2328.

Renggli, S., Keck, W., Jenal, U., and Ritz, D. (2013). Role of autofluorescence in flow cytometric analysis of *Escherichia coli* treated with bactericidal antibiotics. J. Bacteriol. *195*, 4067–4073.

Reynolds, M.G. (2000). Compensatory evolution in rifampin-resistant *Escherichia coli*. Genetics *156*, 1471–1481.

Rosenberg, S.M., and Queitsch, C. (2014). Medicine. Combating evolution to fight disease. Science *343*, 1088–1089.

Schaaper, R.M., and Dunn, R.L. (1987). *Escherichia coli mutT* mutator effect during in vitro DNA synthesis. Enhanced A.G replicational errors. J. Biol. Chem. *262*, 16267–16270.

Shee, C., Gibson, J.L., Darrow, M.C., Gonzalez, C., and Rosenberg, S.M. (2011). Impact of a stress-inducible switch to mutagenic repair of DNA breaks on mutation in *Escherichia coli*. Proc. Natl. Acad. Sci. USA *108*, 13659–13664.

Shee, C., Gibson, J.L., and Rosenberg, S.M. (2012). Two mechanisms produce mutation hotspots at DNA breaks in *Escherichia coli*. Cell Rep. *2*, 714–721.

Shee, C., Cox, B.D., Gu, F., Luengas, E.M., Joshi, M.C., Chiu, L.-Y., Magnan, D., Halliday, J.A., Frisch, R.L., Gibson, J.L., et al. (2013). Engineered proteins detect spontaneous DNA breakage in human and bacterial cells. eLife *2*, e01222.

Shekhar-Guturja, T., Gunaherath, G.M., Wijeratne, E.M., Lambert, J.P., Averette, A.F., Lee, S.C., Kim, T., Bahn, Y.S., Tripodi, F., Ammar, R., et al. (2016). Dual action antifungal small molecule modulates multidrug efflux and TOR signaling. Nat. Chem. Biol. *12*, 867–875.

Skulachev, V.P. (1998). Uncoupling: new approaches to an old problem of bioenergetics. Biochim. Biophys. Acta *1363*, 100–124.

Sung, H.M., and Yasbin, R.E. (2002). Adaptive, or stationary-phase, mutagenesis, a component of bacterial differentiation in *Bacillus subtilis*. J. Bacteriol. *184*, 5641–5653.

Swenson, P.A., and Schenley, R.L. (1974). Respiration, growth and viability of repair-deficient mutants of *Escherichia coli* after ultraviolet irradiation. Int. J. Radiat. Biol. Relat. Stud. Phys. Chem. Med. *25*, 51–60.

Torkelson, J., Harris, R.S., Lombardo, M.J., Nagendran, J., Thulin, C., and Rosenberg, S.M. (1997). Genome-wide hypermutation in a subpopulation of stationary-phase cells underlies recombination-dependent adaptive mutation. EMBO J. *16*, 3303–3311.

Veening, J.W., Smits, W.K., and Kuipers, O.P. (2008). Bistability, epigenetics, and bet-hedging in bacteria. Annu. Rev. Microbiol. *62*, 193–210.

Watanabe, K., Tanaka, M., Yuki, S., Hirai, M., and Yamamoto, Y. (2018). How is edaravone effective against acute ischemic stroke and amyotrophic lateral sclerosis? J. Clin. Biochem. Nutr. *62*, 20–38.

Wimberly, H., Shee, C., Thornton, P.C., Sivaramakrishnan, P., Rosenberg, S.M., and Hastings, P.J. (2013). R-loops and nicks initiate DNA breakage and genome instability in non-growing *Escherichia coli*. Nat. Commun. *4*, 2115.

Woo, A.C., Faure, L., Dapa, T., and Matic, I. (2018). Heterogeneity of spontaneous DNA replication errors in single isogenic Escherichia coli cells. Sci. Adv. *4*, eaat1608.

Xia, J., Chiu, L.Y., Nehring, R.B., Bravo Nunez, M.A., Mei, Q., Perez, M., Zhai, Y., Fitzgerald, D.M., Pribis, J.P., Wang, Y., et al. (2019). Bacteria-to-Human Protein Networks Reveal Origins of Endogenous DNA Damage. Cell *176*, 127–143.

Zhou, Y., and Gottesman, S. (2006). Modes of regulation of RpoS by H-NS. J. Bacteriol. *188*, 7022–7025.

STAR★METHODS

KEY RESOURCES TABLE

REAGENT or RESOURCE	SOURCE	IDENTIFIER
Chemicals and Recombinant Proteins		
ciprofloxacin	MP Biomedicals	Cat# 199020
rifampicin	Research Products International	Cat# 13292-46-1
ampicillin	Sigma-Aldrich	Cat# A9518
doxycycline	Alfa Aesar	Cat# J60422
thiourea	Sigma-Aldrich	Cat# T8656
2,2′ bipyridyl	Sigma-Aldrich	Cat# D216305
edaravone	Sigma-Aldrich	Cat# M70800
isopropyl β-D-1- thiogalactopyranoside	Research Products International	Cat# 156000-5
2-Nitrophenyl β-D-galactopyranoside	Sigma-Aldrich	Cat# N1127
dihydrorhodamine	Life Technologies	Cat# D632
sodium salicylate	Sigma-Aldrich	Cat# 54-21-7
Sytox Blue dead cell stain	Technologies	Cat# S34857
E. coli Sigma S antibody	Neoclone	Cat# WP009; RRID: AB_2564413
E. coli RpoB antibody	BioLegend	Cat# 663903; RRID: AB_2564524
Experimental Models	*Escherichia coli* K12 strains Table S5	N/A
Primers		
rpoB cluster I - FWD	GAC AGA TGG GTC GAC TTG TCA G	N/A
REV	AGG TGG TCG ATA TCA TCG ACT T	
rpoB cluster I - Sequencing	GAA GGC ACC GTA AAA GAC AT	N/A
rpoB cluster II - FWD	TCG AAG GTT CCG GTA TCC TGA G	N/A
REV	GGA TAC ATC TCG TCT TCG TTA AC	
rpoB cluster II - Sequencing	CGT GTA GAG CGT GCG GTG AAA	N/A
ampD - FWD	GTC GGG TGT CAG GGT TAT AG	N/A
REV	CGC TTC AAG ACG ATG ATC AAG	
ampD - Sequencing	ATA AGG TAG AAA CAT GCT ACT CT	N/A
yiaG-mCherry SH – FWD	CCCGGCATTAAGTAAGCAGTTGATGGAATAGAC TTTTATCATG GTTTCCAAGGGCGAGGA	N/A
REV	GCGGGTGATGCAACAATTATTTTTCATATTTATGATT AATGTG TAGGCTGGAGCTGCTTC	

CONTACT FOR REAGENTS AND RESOURCE SHARING

The corresponding author, Susan M. Rosenberg (smr@bcm.edu), is the contact for reagent and resource sharing.

EXPERIMENTAL MODEL AND SUBJECT DETAILS

Escherichia coli (strain MG1655) and isogenic derivatives were used for all experiments.

METHOD DETAILS

Strains, Media, and Growth

E. coli strains used are shown in the Table S5, and the specific strains used in each figure listed in the following section. Bacteria were grown in LBH rich medium (Torkelson et al., 1997) at 37°C with aeration, and additives where indicated at the following

concentrations: ciprofloxacin (cipro, 1–64 ng/mL, Table S1), ampicillin (100 μg/ml), chloramphenicol (25 μg/ml), kanamycin (50 μg/ml), tetracycline (10 μg/ml), rifampicin (110 μg/ml), and sodium citrate (20 mM).

Bacterial Strains Used in Each Figure

Figure 1: (B) MG1655, SMR5223. (C) MG1655, SMR5223, SMR24603, SMR23099. (D) MG1655, SMR5223. (F) SMR5223, SMR11641, SMR11642, SMR5226, SMR21948, SMR23928, SMR11640, SMR23957, SMR23925, SMR23962, MG1655, SMR20479, SMR21338, SMR20475, SMR20467, SMR20477, SMR21321, SMR23974, SMR23930, SMR23982. (G) SMR14334; (H) SMR14334. (I) MG1655, SMR24600. Figure 2**:** (A) SMR24100, SMR24156. (B) MG1655. (C) SMR24096, SMR24134. (D) MG1655. (E) SMR24096, SMR24134. (F) MG1655, SMR20479. (G) SMR24450, SMR24451. (H) SMR14334. (I) SMR24100, SMR24156. Figure 3: (A) SMR24096, SMR14471. (B) SMR24096, SMR24134, SMR14471. (C) SMR24096, SMR24134. (D) MG1655. (E) MG1655. (F) SMR14334. (G) SMR24100, SMR24156. (H) MG1655. Figure 4: (A) SMR24268. (B) SMR24852, SMR24853, SMR24854. (C) SMR24854. Figure 5: (A) SG30013, SG30018, SMR24524, SMR24516, SMR24520, SMR24542, BA701, BA709, SMR24546. (B) SMR24096, SMR24692, SMR24688, SMR24694, SMR24695, SMR24436, SMR24134. (C) SMR24096, SMR24690, SMR24688, SMR24694, SMR24118. (D) SMR24450, SMR24451, SMR24452, SMR24453. (E) CH2046, PM1450. Figure 6: (A) MG1655, SMR24682, SMR24678, SMR24680, SMR5223, SMR24676, SMR24672, SMR24674. (B) SMR24450, SMR24451, SMR24684, SMR24686. (C) SG30013, SMR24539. (D) SMR24096, SMR24134, SMR24725. (E) SMR24100, SMR24156, SMR24705. (F) MG1655, SMR24682. (G) SMR24462, SMR24466. (H) MG1655, SMR21338, SMR20467. (I) SMR24096, SMR24561, SMR24563, SMR24134. Figure 7: (B) SMR24700. (C) SMR24700. (D) SMR24700. (E) SMR24347. (F) SMR24700, SMR24347. (G) SMR24096, MG1655, SMR21774, SMR23984, SMR23985, SMR5223, SMR21772, SMR239990, SMR23991. Figure S1: (D) MG1655, SMR20479, SMR21338, SMR20475, SMR20467, SMR20477, SMR21321, SMR23982. (E) MG1655, SMR20479, SMR21338, SMR24004, SMR5223, SMR11641, SMR11642, SMR24002. (F) SMR24096, SMR24134. (G) MG1655, SMR21938, SMR21940, SMR21946, SMR5223, SMR21911, SMR21913, SMR21919. Figure S2: (A) MG1655, SMR5223, SMR24603, SMR24604, SMR24606, SMR24608, SMR24612, SMR24620, SMR24626, SMR24627, SMR24629, SMR24631, SMR24635, SMR24643, SMR24649, SMR24650, SMR24652, SMR24654, SMR24658, SMR24666, SMR24707, SMR24708, SMR24709, SMR24711, SMR24712, SMR24714, SMR23097, SMR23099, SMR23100, SMR23101, SMR23102, SMR23104, SMR23107, SMR23113, SMR23120, SMR20479, SMR11641, SMR20475, SMR5226, SMR20467, SMR21948, SMR20477, SMR23928, SMR21321, SMR11640, SMR24682, SMR24600, SMR24450, SMR24451, SMR24452, SMR24453, SMR24096, SMR14471. (B) MG1655, SMR816, SMR24603, SMR24604, SMR24606, SMR24608, SMR24612, SMR24620, SMR24626, SMR24627, SMR24629, SMR24631, SMR24635, SMR24643, SMR24649, SMR24650, SMR24652, SMR24654, SMR24658, SMR24666, SMR24707, SMR24708, SMR24709, SMR24711, SMR24712, SMR24714, SMR23077, SMR23079, SMR5880, SMR23081, SMR23087, SMR20479, SMR11641, SMR20475, SMR5226, SMR20467, SMR21948, SMR20477, SMR23928, SMR21321, SMR11640, SMR24682, SMR24600, SMR24450, SMR24451, SMR24452, SMR24453, SMR24096, SMR14471. Figure S3: (A) SMR14334. (B) SMR24096, SMR24134. (C) MG1655, SMR20479. (D) MG1655. (E) SMR24096, SMR24134. (F) MG1655. (G) SMR24096, SMR24134. (H) SG30013. (I) SMR14334. (J) SMR24100, SMR24156, SMR24422. (K) MG1655, SMR24600. (L) SMR24096, SMR24134, SMR24439. Figure S4: (A) SMR14333, SMR14334. (B) MG1655, SMR24100. (C) SMR24096, MG1655. (D) MG1655. (E) MG1655, SMR14471. Figure S5: (A) SMR14471. (B) MG1655. (C) SMR24450, SMR24451. (D) SMR24134, SMR25222, SMR25223. (E) SMR24096, SMR24134. (F) SMR24096, SMR24134. (G) MG1655, SMR24268, SMR24312. Figure S6: (A) SMR24096, SMR14471. (B) SMR24096, SMR14471. (C) SMR24096, SMR14471. (D) SMR24096, SMR14471. (E) SMR24096, SMR14471. Figure S7: (A) SMR24096, SMR14471, SMR24134. (B) MG1655, SMR24024. (C) SMR24268. (D) MG1655. (E) MG1655, SMR21774. (F) SMR24096, SMR24134, SMR24430. (G) MG1655, SMR23984. (H) SMR24450, SMR25224, SMR24451, SMR25225.

Assays for Ciprofloxacin-induced Mutagenesis

Strains and selections

Assays for rifampicin-resistant (RifR) mutants were performed in the WT *E. coli* MG1655 strain, and its isogenic derivatives, and select base substitutions in the *rpoB* gene encoding a subunit of RNA polymerase (see Figure S1A). To assay ampicillin resistant (AmpR) mutants, we used engineered *E. coli* strains developed previously (Petrosino et al., 2002) that mutate to AmpR similarly to most clinically relevant Enterobacterial pathogens. The engineered *E. coli* carry a chromosomal cassette of the divergently transcribed *Enterobacter cloacae ampR* and *ampC* genes in the *attλ* site (parental strain, SMR5223, Table S5). In these cells loss-of-function mutations in the *E. coli ampD* gene confer ampicillin resistance by upregulation of the *E. cloacae ampC* (β-lactamase) gene (Petrosino et al., 2002). The cassette allows *E. coli* to mimic most Enterobacteria, which have *ampR ampC* with their intervening promoters. *E. coli* (and Shigella) differ by having an apparent deletion (relative to most Enterobacteria) that fuses the *E. coli ampC* gene to a constitutive low-activity promoter.

Cipro concentrations used at MAC and in dose-response experiments

Saturated overnight LBH cultures, started each from a single colony, were diluted 1:4x10^6 into 25 mL in a 250 mL flask in fresh LBH broth and incubated at 37°C with shaking for 3–3.5 h, then diluted 1:3 into fresh LBH broth (“no-cipro” controls) or into LBH with cipro at a final “sub-inhibitory” MAC, which causes a final cfu titer of 10% of the titer observed in the no-cipro control. Each strain’s MAC was used in mutagenesis assays (fluctuation tests, below). These concentrations were determined individually for each experimental

strain, and are shown in Table S1. For dose-response fluctuation tests, the final cipro concentrations were 1, 2, 4, 8.5, 10, 12 and 14 ng/ml.

Fluctuation test protocol

For all fluctuation tests, between 10 and 60 independent saturated overnight cultures per strain were assayed as above. From the diluted cultures (above), between 10 and 60 1 mL aliquots were dispensed into 96-deep-well plates or 14 mL tubes as the start of each independent culture. This gives between 10^4 and 10^5 cfu per well/tube. The tubes/plates were incubated at 37°C with shaking. These cultures are independent because no mutants are present at these low numbers of cells. The time of cipro addition to the early log (3-3.5hr) cultures is called time 0. After 24h (RifR) or 48h incubation (AmpR), samples were plated onto LBH agar for determination of total viable cfu titers or selective LBH-agar plates containing rifampicin (110 μg/ml) or ampicillin (100 μg/ml) to select mutants resistant to each drug. LBH-agar plate cfu were counted after 16-24h growth at 37°C. Ampicillin-agar plate cfu were counted after 20-24h growth at 37°C. Rifampicin-agar plate cfu were counted after 44-60h growth at 37°C.

Total and resistant cfu were counted, and mutation rates (mutations per cell per generation, or mutations per chromosome per generation) estimated with the MSS-MLE algorithm using the FALCOR calculator (Hall et al., 2009). The raw mutation rates (Table S2) and their fold induction by cipro-induced were determined as the ratio of the mutation rates of the treated divided by the untreated control samples. Raw rates and fold-induction values for all strains assayed are given in Table S2.

For fluctuation tests performed with addition of reagents that reduce ROS, the final concentrations were 100 mM for thiourea, 0.25 mM for 2,2′-bipyridine, and 100 μM for edaravone. Ten aliquots of log-phase cultures were diluted 1:3 and dispensed into 14-mL tubes with and without chemicals that reduce reactive oxygen and with and without MAC cipro and then grown at 37° shaking for 24h (RifR) or 48h (AmpR) as for the mutagenesis assays.

Gam and GamGFP

For assays in which GamGFP was produced to trap double-strand breaks (DSBs) (Shee et al., 2013), GamGFP was induced from the chromosome using 10 and 20 ng/mL doxycycline in LBH liquid or in plates, as used for determining cfu/ml. Doxycycline was added to cells at their initial 1:4x10^6 dilution and cultures were grown for 3-3.5h and then diluted 1:3 into fresh LBH and fresh LBH with cipro and dispensed into 10 14-mL tubes and grown for 24h (RifR) as described above. Previously, we found that GamGFP production stops the divisions of cells that obtain a GamGFP focus—a DSB the repair of which is blocked by GamGFP (Shee et al., 2013). Because we do not expect rates of spontaneous DSB formation to differ in RifR mutants from their RifS parents, the killing effect of Gam on cells with DSBs is not expected to affect measurements of RifR mutagenesis when Gam is produced.

Plasmids for σ^S artificial upregulation and the empty-vector control were obtained from the mobile plasmid collection (see Table S5), and were induced with 30 μM isopropyl β-D-1-thiogalactopyranoside (IPTG) at the initial 1:4x10^6 cell dilution from saturated cultures into fresh medium, and cultures were grown for 3-3.5h (37° shaking), then diluted 1:3 into fresh LBH and fresh LBH with cipro, dispensed into 10 14-mL tubes and grown at 37° shaking for 24h (RifR) from the addition of cipro, as described above. IPTG was not present in the plates used to determine RifR or total cfu/ml. σ^S production was confirmed by flow cytometry using the *yiaG-yfp* σ^S-response reporter (see below Flow Cytometric Assays for σ^S- and SOS-Response-Regulated Promoter Activity).

Reconstruction Experiments

Reconstruction experiments were performed to verify that differences in cipro-induced mutant cfu titers observed between WT and various mutant strains were not caused by differences in colony-formation efficiency or speed under exact reconstructions of selection conditions: selective plates with varying amounts of isogenic sensitive neighbor cells. From two replicate cultures for each strain, about 100 cfu of ampicillin-resistant *ampRC* Δ*ampD* cells or rifampicin-resistant *rpoB* A1687C, *rpoB* Δ1593–1598, *rpoB* A1547T mutant cells of each experimental strain genotype were mixed with ~10^9 or ~10^8 isogenic sensitive neighbor cells and plated onto ampicillin or rifampicin selective plates, respectively, and their numbers and speed of forming colonies scored. These platings reconstruct the experimental conditions in which mutant cells form colonies scored in our Assays for Ciprofloxacin-induced Mutagenesis. Resistant mutants were also plated alone for reference. We quantified cfu observed after 24 h (ampicillin) or 48 h (rifampicin) at 37°C. Numbers of independent experiments for each given in the Figure S2B legend.

Competition Experiments

Cultures of sensitive and resistant mutants of each experimental strain genotype were mixed at a 50:50 ratio and grown per fluctuation tests, then plated at the end of the growth period on selective rifampicin or ampicillin medium and non-selectively, to obtain the final ratios of sensitive and resistant cfu after growth in competition. Pure cultures were also established as controls. These experiments showed that neither RifR not AmpR mutants is selected (wins the competition, ending at over 50% of cfu), and both are actually significantly counter-selected relative to their sensitive parent strains (Figures 1C and S2A). These data indicate that all of our estimates of the induction of mutagenesis to RifR and AmpR are underestimates. Numbers of independent experiments for each given in the figure legends.

Flow Cytometric Assays for σ^S- and SOS-Response-Regulated Promoter Activity

Quantification of cells that have induced their σ^S or SOS responses, and how much they have, were achieved using engineered chromosomal fluorescence reporter genes and flow cytometry, per Nehring et al. (2016) and Pennington and Rosenberg (2007) for SOS, and per Al Mamun et al. (2012) for σ^S-response activation. We used the *yiaG-yfp* σ^S-response reporter (Al Mamun et al., 2012) and the

Δattλ::P_{sulA}*mCherry* SOS reporter (Nehring et al., 2016) modified from (Pennington and Rosenberg, 2007) in strains grown under fluctuation-test conditions as described for Assays for Ciprofloxacin-induced Mutagenesis, with or without cipro, at indicated concentration(s), and harvested the cells in late log phase or stationary phase. For quantification, flow cytometry "gates" were calibrated, for SOS, using the negative-control SOS-off *lexA*(Ind$^-$), and SOS-response proficient cells, per (Pennington and Rosenberg, 2007), as the dividing place between peaks of the bimodal distribution of SOS-proficient cells at which most cells diverge from the spontaneously SOS-induced fluorescent cell subpopulation, usually at between 0.5% and 1% of cells cultured in LBH broth. With this gate, $\sim 10^{-4}$ of SOS-non-inducible *recA* or *lexA*Ind$^-$ cells cross the gate, scoring as "SOS-positive," per (Pennington and Rosenberg, 2007). For the σ^S response, gates for σ^S-high activity cells were set to the point at which fewer than 0.5% of cells with cipro but without the reporter gene were positive. At this gate fewer than 10^{-3} of Δ*rpoS* cells, which are σ^S-response deficient, cross the gate and would be scored as positive. For all, the percent of the population that scored as positive is reported.

Fluorescence-Activated Cell Sorting

Cell sorting was performed using a FACS Aria II cell sorter (BD Biosciences, San Jose, CA) with a 70-μm nozzle. *E. coli* cells were identified using forward and side scatter parameters, and these were sorted using sterile 1X phosphate buffered saline (PBS) as sheath fluid. After treatment with MAC cipro for 24 hours (RifR) (identical to Assays for Ciprofloxacin-induced Mutagenesis, above), yellow fluorescent protein-positive (σ^S activity, *yiaG-yfp*) and non-fluorescent cells were sorted into 14 mL conical tubes (20-30 × 10^6 negative cells and 3-10 × 10^6 positive cells) and plated on LB agar with and without rifampicin to determine cfu/mL (per Assays for Ciprofloxacin-induced Mutagenesis, above). These data were used to calculate RifR mutant frequencies in the sorted σ^S-high, σ^S-low, unsorted, and mock-sorted populations, the last being cells run through the machine and all cells collected. For Figure 3A, the fold induction of RifR mutant frequency among sorted cells, the cipro-treated mutant frequencies from σ^S-high, σ^S-low, unsorted, and mock-sorted populations were divided by the mutant frequency of unsorted cells grown without cipro in the same experiments. Cells grown without cipro do not have a distinct σ^S-high population—all are somewhat higher than in log-phase cells and not nearly as high as the σ^S-high subpopulation cells after cipro treatment (see Figures S5E and S5G). Control sorts for fluorescence from P_{lac}*cfp*, a negative control for metabolically active cells, and mutagenesis assays, were performed similarly in parallel with the experimental sorts.

HPII Catalase Activity

HPII (σ^S-dependent catalase) activity was measured as described (Iwase et al., 2013). The viable cell titers (cfu/mL) of cells growing in LBH broth were determined at appropriate time points in log or stationary phase. HPI catalase was inactivated by heating 100 μL culture aliquots at 55°C for 15 min. After inactivation, 100 μL 30% H_2O_2 and 1% Triton X-100 (Sigma) were added. After an additional 15 min incubation, the height of bubble formation was measured in millimeters. The millimeters of bubbles were then normalized to cfu/mL of cells. Controls in Δ*rpoS* cells demonstrated that these assays report on σ^S-response-dependent catalase activity.

Microscopy and Quantification of GamGFP (DSB) and TetR-mCherry (Chromosome) Foci

Saturated overnight LBH cultures of cells carrying the chromosomal inducible GamGFP cassette were diluted 1:4x10^6 into 25 mL LBH broth in 250 mL flasks and grown for 3 h. These were then diluted 1:3 into LBH with or without cipro (1-8.5 ng/ml). GamGFP, a DNA DSB-specific binding protein that traps DSBs and inhibits their repair (Shee et al., 2013), was induced in late log phase using 40 ng/mL of doxycycline. After 2 h of induction, cells were fixed with 1% paraformaldehyde and placed at 4°C until microscopy images were taken. For chromosome quantification, saturated overnight LBH cultures of cells containing the inducible TetR-mCherry plasmids and the *tetO* chromosomal array were diluted 1:4x10^6 into 25ml in 250mL flasks and grown for 3 h. These were then diluted 1:3 into LBH with or without cipro (MACs). The TetR-mCherry protein binds to the chromosomal *tetO* array labeling *oriC*-proximal chromosomal units as red foci, and was induced in late log-phase using 2 μM sodium salicylate. After 4h of induction, cells were fixed with 1% paraformaldehyde and placed at 4°C until microscopy images were taken. Images were obtained with an inverted DeltaVision Core Image Restoration Microscope (GE Healthcare) with a 100X UPlan S Apochromat (numerical aperture, 1.4) objective lens (Olympus) and a CoolSNAP HQ2 camera (Photometrics). Captured images for analysis were chosen randomly. The images were taken with Z stacks (0.15-μm intervals) and then deconvoluted (DeltaVision SoftWoRx software) to visualize the whole cell for precise and accurate quantification of foci per Xia et al. (2019). For each experiment, > 400 cells were counted using ImageJ software (NIH) with visual inspection from each independent experiment. Only foci that overlapped with DAPI DNA stain were quantified (≥99% of all foci).

Live Cell Deconvolution Microscopy

Cells were grown as for Assays for Ciprofloxacin-induced Mutagenesis. At 8 hours after the addition of ciprofloxacin (8.5 ng/mL), 4 μL of culture were plated onto 35mm glass bottom cell culture plates. An agar pad containing spent medium from replicate cultures (8.5 ng/mL cipro in cells grown for 8h) was placed on top of the cells, and a glass coverslip placed over the agar pad and sealed with silicon grease to limit evaporation. Images were taken every 1-2 hours for 12 hours with an inverted DeltaVision Core Image Restoration Microscope (GE Healthcare) with a 100X UPlan S Apochromat (numerical aperture, 1.4) objective lens (Olympus) and a CoolSNAP HQ2 camera (Photometrics). Captured images for analysis were randomly chosen. The images were taken with Z stacks (0.15-μm intervals) and then deconvoluted (DeltaVision SoftWoRx software) to visualize the whole cell. For each experiment, > 250 cells were followed to track the activation of the GFP (P_{sodA}*gfp* oxidative stress response) and mCherry (σ^S activity) using ImageJ software (NIH) with visual inspection from each independent experiment.

rpoB and *ampD* Sequencing

A sole RifR or AmpR colony was isolated from each of 24 cipro-treated or 24 control independent cultures and the *rpoB* or *ampD* gene sequenced. RifR *rpoB* mutations occur mostly within two mutation clusters (Reynolds, 2000), and all isolated mutants contained mutations within one of these two sites of clustering (or rarely both sites). *ampD* loss of function mutations confer ampicillin resistance in engineered *E. coli* that carry the *Enterobacter cloacae ampRC* genes in the chromosome, per Petrosino et al. (2002) and Assays for Ciprofloxacin-induced Mutagenesis, Strains and selections. The *rpoB* cluster I and II sites were amplified, as described (Reynolds, 2000), STAR Methods KEY RESOURCES TABLE for primers. The *ampD* gene was amplified using primers described in STAR Methods KEY RESOURCES TABLE. PCR fragments were subjected to Sanger sequencing (GeneWIZ, Massachusetts) to identify insertions, deletions, and/or base substitutions.

Western Analyses of σ^S Protein Levels

Proteins were separated by SDS-PAGE and transferred to 200 polyvinylidine (PVDF) membranes (Amersham Biosciences), blocked with 2% blocking buffer, and probed with polyclonal mouse anti-σ^S antibody (1:700 dilution) (Neoclone). Polyclonal mouse anti-RNA polymerase subunit beta (RpoB) was used to detect RpoB as a loading control in Figure 2F (1:1000) (BioLegend). Goat anti-mouse antibody conjugated to Cy5 fluorescent dye (1:5000 dilution) (Amersham Biosciences) was used to detect the primary antibody-bound σ^S or RpoB protein. Fluorescence was quantified using a Typhoon scanner, with a PMT of 500 and 670BP 30Cy5emission filter, and the bands quantified using ImageJ software (NIH). Quantifications from two or three separate western blots for σ^S are reported, each with band intensities normalized to the values from isogenic WT cells with no cipro treatment run in parallel, and the means ± SEM shown.

Beta-galactosidase Assays

Cells were grown as for Assays for Ciprofloxacin-induced Mutagenesis to equivalent ODs and frozen at −20°C until assays were carried out. Determination of the β-galactosidase activity of the P_{arcZ}-*lacZ*, P_{dsrA}-*lacZ*, *rpoS-lacZ*, and *katG-lacZ* fusions was accomplished using the standard assay described by JH Miller, as previously (Gibson et al., 2010), except that the assays were carried out in 96-well plates to ease sample processing.

Flow Cytometric Detection of Intracellular ROS or GFP and σ^S Activity in Single Cells

Cells were grown in the absence or presence of MAC cipro to early-, late-log, and stationary phase as for Assays for Ciprofloxacin-induced Mutagenesis. The ROS measurement protocol was modified from Gutierrez et al. (2013). Cells were incubated with ROS-staining dye dihyrdorhodamine 123 (DHR) (Invitrogen) for 30 min at 37°C in PBS. After washing twice with PBS buffer, flow cytometry analyses were performed immediately. Gates for ROS-positive cells were set so that < 0.5% of cells treated with cipro without DHR dye were positive. For experiments in which ROS or GFP and σ^S activity were measured, cells were grown in the absence or presence of MAC cipro as for Assays for Ciprofloxacin-induced Mutagenesis (above), then harvested serially from cultures at 4, 8, 12, 16, 24, and 48 hours for ROS detection using DHR or at 12, 16, and 24 hours for ROS detection using the P_{oxyR}*gfp* or P_{sodA}*gfp* transcriptional fusions (Table S5). For ROS detection using DHR, cells containing σ^S-activity reporter *yiaG-mCherry* were collected and ROS detected as green fluorescence, and σ^S activity as red fluorescence. For ROS detection using P_{oxyR}*gfp* and P_{sodA}*gfp*, cells containing both σ^S-activity reporter *yiaG-mCherry* and plasmids carrying the P_{oxyR}*gfp* or P_{sodA}*gfp* reporters, or a promoterless *gfp* parental plasmid Pvector-*gfp*, were maintained with 35μg/mL kanamycin, and used to detect both GFP and red fluorescence. Single color and no-fluorescence controls were also collected at time points for spectral compensation. For the P_{oxyR}*gfp* or P_{sodA}*gfp* transcriptional fusions, gates were drawn so that the promoterless-*gfp* vector Pvector-*gfp* had < 0.5% GFP-positive cells. σ^S high-activity-cell gates were drawn so that < 0.5% of cells without cipro were positive, and MAC cipro-treated WT cells without the chromosomal σ^S-response reporter had fewer than 0.5% scored as positive.

Controls for Appearance of ROS-high Subpopulation Before σ^S-high Subpopulation

In Figure 4A, the ROS-high cell subpopulation is apparent hours before the σ^S-high cell subpopulation, with ROS detected by DHR dye and σ^S activity by mCherry fluorescence from a gene the transcription of which requires σ^S. We can be sure that the appearance of ROS before σ^S activity is not the result of the lag between induction of transcription and appearance of a translated fluorescent protein because the same result is obtained when ROS and σ^S activity are both detected by fluorescence reporters each of which requires transcription and translation Figure 4B. Additionally the lag between induction and appearance of flow-cytometry-detectable fluorescent protein is under 15 minutes (Pennington and Rosenberg, 2007), much less than the lag between ROS-high and σ^S-high cells (Figure 4).

Experimental Definition of Cipro-induced Multi-chromosome Cell Filaments

Without cipro only 1% ± 0.7% of exponential (16h post-cipro) WT cells have four or more chromosome copies (Figure 7C), so we defined a multi-chromosome cell as those with ≥ 4 chromosome copies. With cipro, 33% ± 2% of WT cells have ≥ 4 chromosome copies (Figure 7B). By contrast, Δ*sulA* cells show much reduced cell length and chromosome content (Figures 7D–7F).

Mathematical Modeling of Cipro-induced Multi-chromosome Cell Filaments

In our model, a population of microbes is exposed to severe external stress (e.g., antibiotics), and two strategies are available: either growing into "filament" cells, that can contain multiple DNA copies, or reproducing individually. We consider a case in which resistance to the external stress can be acquired by a single mutation, with baseline rate μ, and deleterious mutations occur at many other loci, with the number of deleterious mutations per replication following a Poisson distribution with average λ. We assume that during the external stress the basic mutation rates of all cells (both μ and λ) increase A-Fold, and mutation rates in filament cells are further increased B-fold relative to non-filament cells.

We denote by s and δ the selection coefficients against the external stress and each deleterious mutation, respectively. We denote by I_a the level of adaptation to the external stress, where $I_a = \begin{cases} 1 & adapted \\ 0 & not\ adapted \end{cases}$. The fitness (modeled here as the probability to replicate) of an individual that possess n deleterious mutations is thus $\omega(I_a, n) = (1-s)^{1-I_a} \cdot (1-\delta)^n$. In the filament population, we assume that DNA copies in the same cell filament share gene products, and that deleterious mutations are recessive. Once a genome copy within the filament acquires the beneficial mutation that confers resistance to the major stress, it buds out of the filament, and begins to duplicate regularly (in proportion to the number of deleterious mutations it possesses).

We follow the two strategies for k replication cycles, starting from a population that doesn't carry any deleterious mutations nor is adapted to the external stress. In the filament population the cells duplicate their genome without dividing and have up to 2^k DNA copies. Because the populations begin without any deleterious mutations, we neglect filaments in which all DNA copies share the same deleterious mutation. Therefore, the fitness of DNA copies in the filament population is affected only by the external stress, while in the non-filament population the fitness of each DNA copy (or cell) is affected both by the external stress and by the number of deleterious mutations it carries. After k replication cycles the filaments divide to cells, each containing a single DNA copy. We then compare the population size and fitness, the proportion of adapted individuals, and the distribution of deleterious mutations, between the filament population and the non-filament population.

Parameter values in Figure 7H: $\lambda = 0.003, \mu = 6 \cdot 10^{-7}, \delta = 0.03, A = 100, k = 4$. In the left and middle panels we use $B = 4$ and $s = 0.9$, whereas in the right panel B is the value on the x axis. The value $B = 4$ is derived from empirical results presented in Figure 7G, in which we see that during antibiotic stress the mutation rate of cells that do filament (WT) have a fold-increase of ~4 relative to non-filamented cells.

The model tests the effect of filaments on evolvability, where mutation serves as the variation mechanism. However, if chromosomes in filaments also experience recombination, then the system corresponds to the case of Fitness-Associate Recombination (FAR) (Hadany and Beker, 2003b) – the less fit chromosomes experience higher recombination rate then the fitter ones. Previous work has shown that this mode of recombination results in increased mean fitness and improved adaptability (Hadany and Beker, 2003a).

Parameters:

Beneficial mutation rate $\sim Ber(\mu)$
Deleterious mutation rate $\sim Poisson(\lambda)$
A – stress-induced increase in mutation rate
B – filament cells fold increase in mutation rate relative to non-filament cells
s – selection coefficient of the antibiotic
δ - selection coefficient of each deleterious mutation (multiplicative model)
k – number of replication cycles

Measurement of High-Dose Cipro Antibiotic Activity

Cells were grown to log phase OD_{600} ~0.5, then cipro (1.5 μg/mL) with or without edaravone (100μM), and were harvested 0.75, 1.25, 2.25, and 3 hours later to determine cfu/mL. Cells were washed twice with PBS and then assayed for viable cfu.

Nalidixic-Acid Test for Heritable Hypermutability

Tests for heritable mutator phenotype were as described (Torkelson et al., 1997). Ten independent cipro-induced RifR mutant isolates, each with a different mutation, were grown in parallel with control WT (non-mutator) and *mutS* mismatch repair-defective (mutator) strains each in duplicate independent cultures. 100μL of each saturated overnight culture was spread onto an LBH agar plate. After 10 minutes, dry nalidixic acid powder was spotted onto each plate using a capillary tube. The plates were incubated for 24 hours at 37°C, after which the number of microcolonies in the zones of inhibition were counted, and compared with the positive (*mutS*) and negative (isogenic WT) controls.

Flow-Cytometric Detection of Dead Cells

Cells were grown in the presence of MAC cipro per Assays for Ciprofloxacin-induced Mutagenesis (above), and harvested serially from cultures at log phase (4 and 12 hours) and stationary phase (24 hours) for dead cell detection using SYTOX blue dead cell stain. Cells were stained according to manufactures recommendation. Cells were incubated with SYTOX blue dye (1μM) for 30 minutes at

room temperature and flow cytometry analyses were performed immediately. As a positive control, cells were incubated in 95% ethanol for 10 minutes before staining. Positive gates for dead cells were set so that < 0.2% of undyed cipro-treated cells were positive, at which 90% ± 5% of the SYTOX-blue dyed positive-control ethanol-treated cells were positive.

Statistics

Statistics were performed in Microsoft Excel or GraphPad PRISM. For comparisons of two groups, a two-tailed Student's t test was used if data were normally distributed and homoscedastic. For comparisons of 3 or more groups, ANOVA with Tukey post hoc test was used if data were normally distributed and homoscedastic, otherwise a Kruskal-Wallis non-parametric test was used. For mutation rates and ratios, which are not normally distributed, natural-logarithm transformed data were used to calculate 95% confidence intervals (CIs) as well as performing statistical significance tests. 95% CIs appear in bar graphs as error bars that are not symmetrical above and below the top of the bar.